Low Temperature Fluidized Bed Coal Drying:

Experiment, Analysis and Simulation

By:

Tahere Dejahang

A thesis submitted in partial fulfillment of the requirements for the degree of

Master of Science

In

Chemical Engineering

Department of Chemical and Materials Engineering

University of Alberta

Abstract

Drying kinetic of Canadian lignite was studied in a pilot scale fluidized bed dryer using low temperature air (T≤70 ˚C). Minimum fluidization velocity was calculated and applied to the experiment. Samples showed poor fluidization due to large particle size (1-2.8 mm) and density (1400 kg/m^3). The effect of drying parameters was studied experimentally. Gas temperature showed a great effect on increasing drying rate in the constant drying period and low effect in the falling rate period. Increasing gas velocity proved to be poorly effective in drying due to low fluidization. Smaller particle size led to higher drying rate. Drying curves were curve fitted to available kinetic models in the literature and logarithmic model showed the best fit. Diffusion coefficient, activation energy and pre-exponential factor of lignite drying were calculated and showed good agreement with reported values in the literature. CFD analysis was carried out in Ansys-Fluent 14.0 and tuning the solid-fluid exchange coefficient, the constant rate drying period was successfully simulated. Spontaneous combustion kinetics of Canadian lignite was studied experimentally and analytically.

Dedicated to my beloved:

*"**Mother**"*

....

Acknowledgement

I would like to thank my kind supervisor Dr. Gupta for his guidance and patience and mention how grateful I am to Dr. Nikrityuk for his support and help in the course of this thesis.

My gratitude extends to all our group members specially Dr. Mehdi Mohammad Ali Pour for their help and support.

Finally, I would like to thank C^5MPT and department of chemical and material engineering staff for their cooperation which made this project possible.

List of Figures

List of Tables

Table of Contents

Chapter 1: Introduction

1-1. Coal structure and formation

Coal is an organic composition of mainly carbon, oxygen and hydrogen. It is a fossil fuel which with almost 109 years of remaining in the whole world is far more abundant than oil and gas. While it can be found in almost all countries, the largest reserves include the US, Russia, China and India. Over 6185 million tonnes (Mt) of hard coal and 1042 Mt of brown coal/ lignite is currently produced worldwide. Coal is formed by the consolidation of vegetables between rocks under pressure and heat over millions of years [1].

Lignite (brown coal) is the lowest rank of coal because of having a low heating value and high moisture content. This low energy density and relatively high moisture content makes it economically inefficient to transport, thus, mostly burnt in power plants situated near the area where it is mined [2]. However in future, lignite can have other applications because of some advantages it has over black coal; including low mining cost, high volatile content and reactivity and low mineral matters such as sulfur and nitrogen [3].

China, Germany, Russia, Australia, the US and Canada are among countries mining lignite [2]. Table 1-1 shows the top 10 Brown coal producers of 2013.

Table 1-1: top 10 brown coal producers of 2013 [1]

Germany	183 Mt	Australia	Germany
Russia	73 Mt	Greece	Russia
USA	70 Mt	India	USA
Poland	66 Mt	Czech Republic	Poland
Turkey	63 Mt	Serbia	Turkey

1-2. Canada's coal reserves

In Canada, with 6.6 billion tonnes of recoverable reserves, coal is certainly the most abundant fossil fuel. Types of Canada's coal deposits include bituminous coal, sub-bituminous coal, lignite and anthracite. West provinces contain more than 90 % of the coal deposits which along with the oil-sand deposits and access to the west coast ports, provide a great advantage for the country.

Canada has 24 coal mines in total which are in British Colombia, Alberta, Saskatchewan and Nova Scotia [4]. In Alberta, coal mining in started in 1800s. The province contains 70 % of the country's coal deposits. Alberta spends more than 25 million tonnes of coal for electricity generation annually. Alberta coal has low sulphur content and thus produces less pollutants compared to many other coals around the world [5].

1-3. Importance of lignite upgrading

In comparison to bituminous coal, lignite burning power plants have lower efficiency which is due to high moisture content of lignite. When wet coal is burnt in a power plant, a large portion of the fuel's heat input (20-25%) is spent on evaporating the water contents [6], which reduces the plant efficiency significantly. High moisture also increases the transportation costs as well as stack flue gas flow rate and the risk of spontaneous combustion [3].

Apart from the economic issues of burning low rank coal, a number of environmental issues arise when using coal as a fuel. Coal is a major source of releasing greenhouse gases (GHG) and toxic minerals to the atmosphere. The greenhouse gases emitted by coal burning power plants include Carbon Dioxide (CO_2), Carbon Monoxide (CO) and Methane (CH_4) [7]. At present the CO_2 produced by burning lignite for generating a MWh electricity is one third

more than that of black coals [6]. If coal moisture content is reduced from 60% to 40%, a relative reduction of 30% in the CO_2/MWh will be resulted [8].

These environmental issues have motivated researchers and industries to look for alternatives for coal and other fossil fuels. Innovative techniques and materials like biomass were suggested, but high production and installation costs, as well as maintenance expenses are barriers stopping investors from applying these new technologies. This signifies the importance of producing low moisture clean coal to feed power plants which are environmental friendly [9].

Countries with largest lignite reserves like Germany, Australia and the U.S are the pioneers in searching for effective coal-dewatering and drying techniques [10].

The amount, distribution and type of bounding of water in coal are factors determining the ease of its removing from coal. Coal matrix is composed of small and large capillaries which control the transport of the gases (water, oxygen etc.) through it [11]. Understanding the characteristics of the coal which is to be dried is the key factor in choosing the right technique and designing efficient setup for water removal.

The majority of the developed techniques use high-grade heat to dry coal or require complex and expensive equipment, increasing the cost of thermal drying, and thus preventing the application of these techniques in large industrial scales [12].

Moreover, use of carbon capture technology at power plants which burn low-rank, high-moisture coals signifies the need for efficient, inexpensive coal

drying methods to recover a portion of the efficiency loss due to the compression of carbon dioxide (CO2), so that, future power plants, employing CCS, would benefit from thermally dried coal [12].

1-4. Types of water in coal

The nature and type of water and its boundings in coal have been studied in the literature and different classifications have been suggested. It is widely accepted that water can be as a free or bound phase in coal [13]. In the primary researches, water in coal was classified as freezable and non-freezable. Freezable water was the larger fractions of water in the coal structure which was able to crystallite and create ice, while non-freezable water referred to adsorbed water on the internal surfaces or the water in small pores which was incapable of creating crystal ice [14]. Another classification by (Allardic and Evans 1971) suggested 2 types of water in coal: chemically adsorbed water which can only be removed by temperature increase and thus thermal decomposition, and water which can be removed by evacuation. Increasing the temperature will result in progressive removal of the first moisture type.

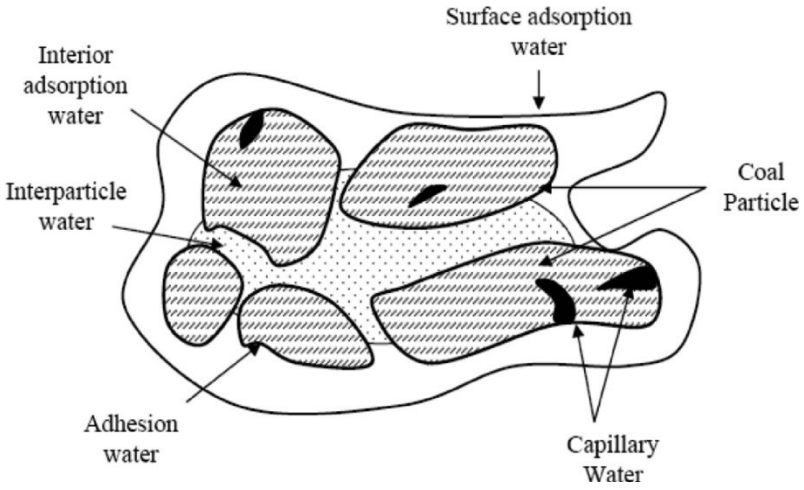

Figure 1-1: types of water in coal [15]

More elaborate classification by Allardic and Evans was suggested in 1978 [15]. It involves 5 possible types of water in coal:

(1) *Interior adsorption water*: water trapped in micro pores and micro capillaries during the formation of coal;

(2) *Surface adsorption water*: A layer of water molecules on the coal particle surface (chemically bounded);

(3) *Capillary water*: water deposited in the particle capillaries;

(4) *Inter-particle water*: water found in the crevices among two or more particles;

(5) *Adhesion water*: A film of water in the surface of a coal particle.

Water in type (4) and (5) which is known as surface water can be removed by mechanical force. A portion of type (3) can also be removed mechanically if the sizes of the capillaries are large enough. Water types (1) and (2) however, can only be removed thermally. Figure 1-1 elaborates these five different types graphically.

1-5. Scope of the study

In this study, drying process of Canadian lignite in a fluidized bed drier is investigated. The effect of different drying parameters such as temperature or particles size, as well as the kinetic of drying is studied. The drying process is simulated mathematically and using CFD method and the chance of spontaneous ignition of dried coal is investigated experimentally and analytically.

Chapter 2: Literature review

2-1. Necessity of coal drying

Coal is a cost-effective fuel for power plants and industries due to its high abundance and low cost. Around 45 % of the world's coal reservoirs consist of lignite, a cheap coal type, low in sulfur but high in moisture (25-40%), resulting in a low calorific value compared to other coal types [16], [17]. Great tendency for spontaneous combustion, and high transportation costs are other disadvantages of lignite, making it undesirable for industrial processes. Moisture reduction can increase the quality and efficiency of coal to a desirable amount for different processes. However, due to high amount of moisture in lignite, drying requires a large amount of energy [17]. Table 2-1 shows the approximate ranges of moisture content of coal for different processes.

Table 2-1: approximate ranges of moisture content of coal required for various processes[17]

Type of coal	Usage of coal	Optimum moisture content (%)
Hard Coal	Coking processes (based on the ramming method)	8-12
	Coking processes (based on the Charring method)	<8
	Low temperature carbonization process	~0
	Hydrogenation process	~0
	Coal Combustion process in a pulverized fuel fired furnace	<2
Brown Coal	Briquetting process	8-18
	Gasification process	5-12
	Low temperature carbonization process	<15
	Hydrogenation process	~0
	Coal combustion process in a pulverized fuel fired furnace	12-15

2-2. Coal drying methods

Drying is defined as reducing the water content of coal to a desired level. This can be done through (i) evaporating drying or (ii) non-evaporating drying.

2-2-1. Evaporating drying

When the water content of the coal is transferred into gas phase to be removed, the process is called evaporating drying [10]. This method mostly uses superheated steam, hot air or combustion gases. Typical dryers working based on this principle include: fixed and fluidized beds, rotary kiln and entrained systems [17]. Generally, in the evaporative drying methods, Coal is introduced into a rotary vessel where superheated steam is applied. The discharged steam is partially condensed, just enough to subtract the added water by the drying process, with the remaining steam being reheated to enter the cycle again [10]. Besides increasing thermal efficiency of coal, this method reduces the risk of spontaneous combustion of coal by decreasing coal reactivity in the presence of oxygen [18].

2-2-1-1. Rotary drum steam tube dryer

This evaporating drying technique is currently used by industries in Germany and India. It includes a steam drum with coal passing through the tubes inside the drum. This method reduces the risk of fire by dried coal significantly [10].

2-2-1-2. Integrated flash mill drying systems

This method is used for ground brown coals. The brown coal is crushed into powder in a “beater” mill and is exposed to hot flow gas. The gas is then recycled from the furnace exit. In another similar technology, the gas temperature is increased by burning some coal or natural gas and then is fed to the mill [10].

2-2-1-3. Fluidized bed dryer

Fluidized beds consist of a bed of particles exposed to an upward pressurized fluid which results in particles showing fluid-like behaviour. They are widely used in food and other industries dealing with granular solids [19].

2-2-2. Non-evaporating drying

Non-Evaporating drying includes methods distracting water in coal by applying pressure and mechanical forces. Examples include: Fleissner Process, K-Fuel, mechanical thermal expression (MTE) and hydrothermal dewatering (HTD). These methods mainly use heat and pressure to increase the heat value of coal and reduce impurities such as mercury and sulfur dioxides and nitrogen oxides in coal physically and chemically [10][17].

2-2-2-1. Fleissner Process

In this process lump coal particles, without being crushed into smaller sizes, can be economically dried. Coal lumps are placed in a batch autoclave and heated in 180-240 °C steam under 400 pounds of pressure. The steam carrying the moisture leaves the dryer and the remaining moisture is removed using a vacuum pump. The dried lump contains less than 10 % moisture and a heating value of 10000 Btu/pound. It can be ground to powder form easily and even burns efficiently in the lump form. Several industries in Europe use this technique [10].

2-2-2-2. Hydrothermal dewatering

Hydrothermal dewatering is a process in which coal is heated up under pressure to temperatures above 180 °C. In such process physical and chemical mechanisms release an increasing amount of water from coal. In hydrothermal dewatering hot water, instead of steam, is utilised as the heating medium. The

pressure is kept high enough to make sure water in coal remains in the liquid form [20].

2-3. Fluidized bed

Fluidized beds are widely used in different industrial processes including drying, cooling, granulation, coating etc. They can be used for both heat sensitive and non-heat sensitive materials. In coal industry, fluidized beds are used in processes such as drying, gasification and de-volatilization. Fluidized bed dryers (FBD) are useful for drying powders, granulates, agglomerates, and pellets in the size range of 50 to 5000 μm. Particles out of this size range are either too small or too big to fluidize and may require additional forces, i.e. vibration, to fluidize[21], [22].

2-3-1. Fluidization definition

When an upward fluid is passed through a bed of particles, due to the frictional forces between the fluid and the particles, fluid pressure will decrease. Increasing the fluid flow will increase the pressure drop up to a certain point where a small reduction in the pressure drop is observed (figure 2-1). For air superficial velocities larger than that no more increase in the pressure drop will be observed. The velocity at which the pressure drop stops increasing is called the minimum fluidization velocity, where the drag force applied to the particles will be equal to the apparent weight of the particles. This leads to particles being lifted slightly by the fluid and the bed is considered fluidized [23].

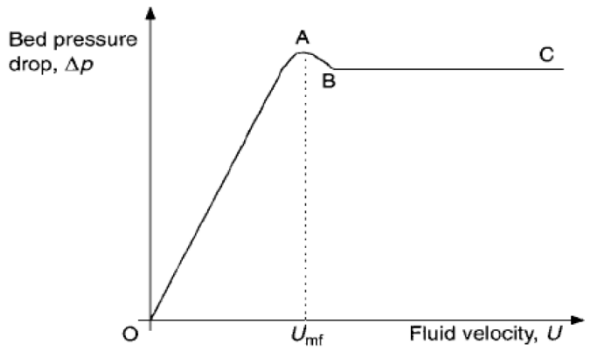

Figure 2-1: pressure drop vs. fluid velocity for packed and fluidized beds [23]

2-3-2. advantages and disadvantages

Some of fluidized bed advantages are:

- high surface area contact between solid and fluid particles
- Quick heat and mass transfer between solid and fluid particles
- Fast particle mixing
- Low maintenance cost [24], [19], [9].

And a few disadvantages include:

- Not sustainable for particles with low sphericity or wide particle size range [17]
- Solid particle erosion due to solid-solid and solid-wall collisions
- Back mixing [25]

To overcome the disadvantages of fluidized beds, several solutions have been proposed. Installing mechanical vibration to the fluidized bed dryer is one of the solutions which increases the uniformity of the process and has been accepted and used by industries [24].

2-3-3. Geldart Powder classification

Geldart (1973) classified materials in terms of their fluidization behaviour into four categories:

Group A:

Materials with a small mean size (less than 30 μm) and/or low density (less than 1.4 g/cm^3) are classified in this group. They are easily fluidized and

slowly collapse when the gas supply is cut off. Face centred cubic catalysts are among this group.

Group B:

This group contains materials in size range of 40-500 μm with a density in range of 4-1.4 g/m^3. Bed expansion is small in this group and it collapses immediately when the air supply is cut off. Bubbles will be formed at air supply velocities a little above fluidization. Sand is the most typical example of this group.

Group C:

Cohesive fine powders belong to this group. Fluidizing this group of materials is very difficult because they lift in plugs of small channels due to their inter-particle attractions being greater than the force applied by the fluid. Flour and cosmetic powders belong to this group.

Group D:

Very large or very dense materials belong to this group. Fluidizing this group is difficult and solid particle mixing is quite poor. Vegetable grains such as bean and coal (including lignite) belong to this group of powders.[9][26]

2-3-4. Fluidized bed equations

2-3-4-1. bed pressure drop

As explained above, fluidization happens when the upward drag force applied on particles from the fluid equals the apparent weight of particles. Righting the force balance in this situation leads to:

$$\text{Fluid pressure drop across the bed} = \frac{particle\ weight - upthrust\ on\ particles}{bed\ cross\ section\ area}$$

Or

$$\Delta p = \frac{HA(1-\varepsilon)(\rho_p-\rho_g)g}{A} = H(1-\varepsilon)(\rho_p-\rho_g)g \quad (2\text{-}1)$$

Where:

H: bed height in (m)

A: bed cross section area (m^2)

ρ_p: Particle density in (kg/m^3)

ρ_f: Fluid density in (kg/m^3)

ε: Bed voidage (dimensionless)

Knowing the bed voidage and particle and gas properties the pressure drop can be calculated.

2-3-4-2. Minimum fluidization velocity

Minimum fluidization velocity U_{mf} is the air supply superficial velocity at which the fluidization occurs. Below this velocity a packed bed is obtained and above that bubbling or spouting bed is reached. U_{mf} increases with particle size and density as is directly affected by the fluid properties [23].

To write an expression for the U_{mf} we can equate the pressure loss equation of a fluidized bed (equation 1) with that of a packed bed. Using this method and taking some assumptions Wen and Yu (1966) produced an equation in the form of:

$$Ar = 1652Re_{mf} + 4.51Re_{mf}^{1} \qquad (2\text{-}2)$$

In equation 2-2, Ar is the dimensionless number known as Archimedes number defined as:

$$Ar = \frac{\rho_g(\rho_p - \rho_g) g\, d_p^3}{\mu_g^2} \qquad (2\text{-}3)$$

And Re_{mf} is the Reynolds number at the fluidization velocity:

$$Re_{mf} = \frac{U_{mf}\rho_g d_p}{\mu_g} \qquad (2\text{-}4)$$

Wen and Yu correlation can also be expressed in the form:

$$Re_{mf} = 33.7[(1 + 3.59 * 10^{-5}Ar)^{0.5} - 1] \quad (2\text{-}5)$$

Valid for spheres larger than 100 µm in the Re_{mf} range of 0.01-1000 [23].

For particles smaller than 100 µm Beayens and Geldart correlation (1974) can be used:

$$U_{mf} = \frac{(\rho_p - \rho_f)^{0.934} g^{0.934} D_p^{1.8}}{1110\mu^{0.87}\rho_f^{0.066}} \quad (2\text{-}6)$$

2-4. Drying kinetics

Studying drying kinetics and characteristics of coal provides important data to be able to pick the most efficient drying technique with the optimum setup built based on that technique. Before employing the setup in the industrial scale, a laboratory scale setup and analysis is required to characterize the whole process under a well- controlled environment [27].

2-4-1. Effect of drying parameters

Vorres [28] and Tahmasebi et al [29] used a thermogravimetric analyzer to study the drying behavior of Wyodak subbituminous coal and Chines lignite respectively. Vorres included that the rate of moisture removal in the sample is affected by the drying temperature, inlet gas flow rate and the sample size. Wang et al [30] reported that if the air flow temperature is increased with a constant rate, weight loss will show a sharp decrease in the first minutes, and then a gradual decrease will be observed till the end of the experiment. Zhao et al [24] investigated the effect of drying conditions on a vibration fluidized bed and concluded that higher frequency and lower bed height were favorable for drying.

2-4-2. Modeling Kinetics

C.Srinivasakannan and N.Balasubramanian suggested a simplified equation to model the constant rate period of drying in a batch fluidized bed. The model divides the bed into dense and bubble phases. Using the characteristics of the materials and the bed shape, it predicts the drying rate of the constant rate period. They compared the predicted drying rate with the experimental results of different materials in different conditions (gas velocity, solid hold-up, bed shape and diameter etc.) and found that the model is in satisfactory agreement with experimental data [31].

Chandran et al [32] introduced a simple model to predict both the constant and falling rate of drying in a fluidized bed. They assumed that the falling rate is linear with starting point at the critical moisture content and ending point at the equilibrium moisture content. Their model predicts the moisture content of the bed material at any time by knowing the initial, critical and equilibrium moisture content as well as the drying rate coefficient R, which is expressed as the weight of water evaporated per unit weight of dry solid.

Edward K. Levy et al [33] studied the drying of coal in a bubbling fluidized bed. They used the conservation of mass and energy and wrote an ODE for coal moisture and bed temperature as a function of time. Solving the ODE numerically and comparing the results with the experiment results of a high moisture sample in the bed, showed good agreement between the two sets of data.

Ciesielczyk et al [34] assumed that heat delivered to the particle is entirely used to remove the moisture and the particle surface is completely covered with the moisture. They also assumed that moisture removal only occurs at the

external surface of the particle and that the temperature of the particle is the wet bulb temperature. They wrote an expression for the drying rate as a function of dry solid mass, specific surface area, solid holdup, concentration gradient and mean mass transfer coefficient. To calculate the mean mass transfer coefficient they used the bubbling bed model.

Syahrul, S et al [35] studied mass, energy and entropy balance of fluidized bed dryers with corn and wheat particles. They studied the thermal efficiency of the bed under different drying conditions such as initial moisture content of the particles, air flow rate etc.

Cai et al [36] presented a general empirical kinetic model for solid state reactions. Their proposed model is $f(\alpha) = \alpha^m(1 - q\alpha)^n$ (m and n are empirical coefficients), where α is the conversion degree in the form of:

$$\alpha = \frac{W_i - W}{W - W_f} \qquad (2\text{-}7)$$

Where:

W_i: initial weight of solids
W: weight of solid at any time
W_f: final weight of solid at the end of the reaction
And f(α) is the kinetic model in differential form. They showed that other kinetic models in the literature can be fitted with their model by calculating proper values for m, n and q in each case. Kang et al [37] studied these kinetic models validity in predicting isothermal and non-isothermal drying of Indonesian coal and concluded that phase boundary reaction in the form of $f(\alpha) = 1 - (1 - \alpha)^{1/3}$ was the best fit for drying Indonesian coal mechanism in an isothermal fixed be reactor.

Burgschweiger et al [38] studied the drying kinetics of a single particle as well as a bubbling fluidized bed of the particles. They believed batch fluidized bed drying curves could be predicted using the single particle and material equilibrium data and their developed model. They derived their model by writing mass and energy balance for the suspension gas and bubbles as well as energy balance for the bed walls. They used van Meel normalization approach but defined a modified normalized drying rate with a mass flux with a sorptive driving force term. Their model coped well with experimental data of single particle drying and batch fluidized bed drying.

Tahmasebi et al [29] and studied lignite drying kinetics using thermogravimetric method. Using the data obtained from the experiment they calculated the apparent diffusion coefficient and activation energy of drying lignite. Mirzaee et al [39]used the same method for drying of apricot in a packed bed.

2-5. CFD modeling

CFD modeling is a very useful numerical method to help optimize processes and improve energy efficiency of industrial cycles [40].

Azizi et al [41] used CFD method to model a spouted bed of glass particles. They used multiphase Eulerian-Eulerian approach based on kinetic theory and using Gidasow's drag model for predicting gas-solid momentum exchange. They studied the effect of solids mass fraction as well as gas flow rate on the distribution of pressure along the spouted bed.

Roman et al [40] used CFD to study heat and mass transfer for drying of grains in a spouted bed. They used Eulerian-Eulerian approach and the applied

heat and mass transfer models using user defined files (UDF) to Fluent 6.1. They concluded that their model predicts mass transfer, Nusselt and Sherwood number accurately but is poorly successful in predicting heat transfer.

Jamaleddine and Ray [42] studied drying of sludge in a cyclone dryer using CFD analysis. They wrote a UDF to simulate constant and falling rate drying periods. The hydrodynamics analysis showed a nun-uniform particle distribution across the dryer. Moisture content, temperature, and velocity were monitored and the model showed a good degree of success in predicting the process.

2-6. Coal spontaneous combustion

Spontaneous combustion of coal has been a serious problem for coal producers and users industries [43]. This phenomenon can result in disastrous economic losses and casualties. Spontaneous combustion happens due to the low temperature oxidation of coal particles. As this process is exothermic, if proper ventilation is not provided, the coal temperature can increase to a point when combustion occurs [44].

Yongliang et al [45] calculated the shortest period of coal spontaneous combustion on the basis of oxidation heat release and coal thermal capacity at different temperatures. They showed that the shortest spontaneous combustion period increases when oxidation absorption is decreased and the activation energy is increased.

Qi et al [46] used DSC experiments to observe the heat behaviour of coal to determine the kinetic parameters and predict the oxidation process. Their study successfully predicted temperature profile of coal in the self-heating

process. Zhao et al [47] used the same DSC instrument as Qi et al and measured activation energy of spontaneous combustion for cotton. Using the Semenov model, they calculated the self-heating oxidation temperature (SHOT) of cotton in different heating rates.

In this study, data obtained from fluidized bed dryer is analyzed using the same apparent diffusion approach used by Tahmasebi [29] and Mirzaee [39]. This method uses the conversion and time data and does not require coal particles temperature which is difficult to measure during the experiments in the bed. CFD modeling is carried out to model the drying process using a constant rate input, and spontaneous combustion risk of Canadian lignite is studied in a TGA-DSC with the same approach as Zhao [47] and Qi [46].

Chapter 3: Setup and Experiments

3-1. Material

The coal sample used in this study is Boundary Dam lignite. Samples were sieved and kept sealed before and after experiments. The proximate analysis of Boundary Dam coal was measured using a Leco TGA701 thermogravimetric analyzer and is presented in table 3-1.

Table 3-1: Proximate analysis of Boundary Dam coal

Fixed carbon%	Moisture %	Volatile matter%	Ashe%
23.4	21	40.5	13.4

3-2. Material density measurement

The particle density used in fluidized beds is the apparent density defined as particle mass divided by its hydrodynamic volume. This volume is the one seen by the fluid and includes the particle and its open and close pores. This density is different from the absolute density which accounts for the real volume of the particle (apparent volume minus the pores). Measuring the apparent density of porous materials is not an easy procedure because common methods measure the absolute density [23]. In this study the apparent density of coal samples was measured using water displacement method [48]. A bottle of known weight was filled with an amount of water with measured weight. A small number of coal particles were weight measured and added to the bottle. The change in the water level was written down immediately, before water diffuses into the particles pores. The measured density for Boundary Dam coal was 1400 kg/m^3.

3-3. Fluidized bed setup and procedure

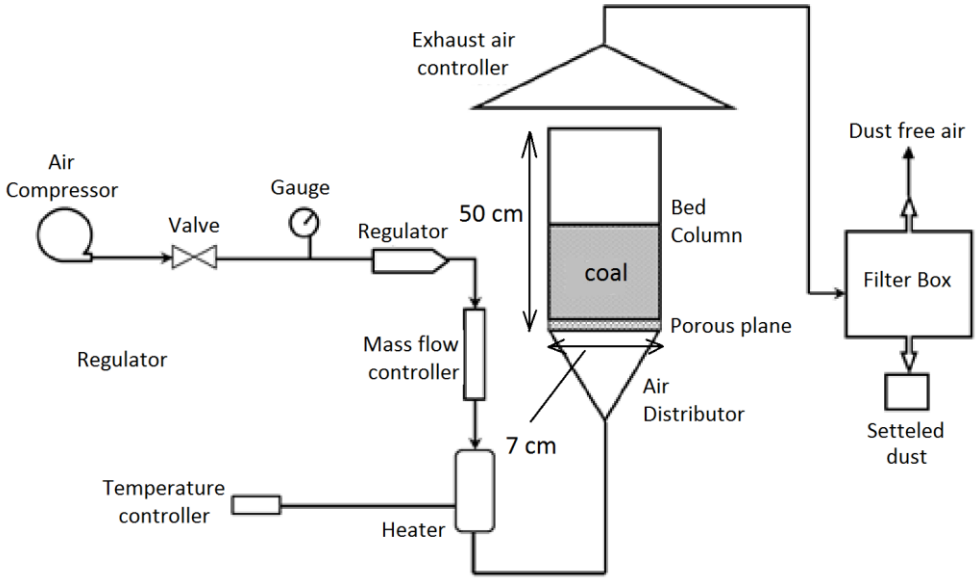

Figure 3-1: Fluidized bed setup for coal cleaning [49]

Figure 3-2: Fluidized bed

Experiments were carried out using the setup schematically depicted in figure 3-1. In the experiment process first air is pumped into a mass flow rate controller to be set to the desired mass flow rate. Air is then heated up in a heater controlled by a temperature controller. The temperature controller takes the heater temperature by a thermocouple and adjusts the voltage to heat the heater to the desired temperature. Hot air leaves the heater and enters the bed

through a porous distributer to keep the air flow uniform across the bed entrance. After the desired temperature is reached, a certain amount of coal is introduced to the bed and the experiment starts. The air flow rate is stopped at certain time intervals and the weight of the whole bed is measured using a microbalance. The experiment continues until no significant change is observed in the bed weight. Subtracting the weight of the empty bed from the measured weight values, the mass of samples in the bed is calculated at each time interval.

3-4. Thermogravimetric procedure

Lignite samples were tested in a Leco TGA701 thermogravimetric analyzer for 10 hours. Air with a flow rate of 7 ml/min was continuously purged into the instrument chamber at isothermal conditions. Samples weight was measured and recorded constantly during the experiments.

Chapter 4: Results and discussion

4-1. Effect of drying conditions on drying rate in Fluidized bed

4-1-1. Effect of inlet gas temperature

In order to investigate the effect of the inlet gas temperature on the drying behavior of Boundary Dam coal, tests with T_{air}=20 °C and T_{air}=50 °C and T_{air} =70 °C were carried out in the bed. The sample size was 1-1.7 mm, the mass of input sample was 100 gr (±5 %) and the initial moisture was 21 % (g of water /g of wet coal) with air flow rate of 90 lit/min (corresponding minimum fluidization velocity, see Appendix A). Figures 4-1 and 4-2 show the test results.

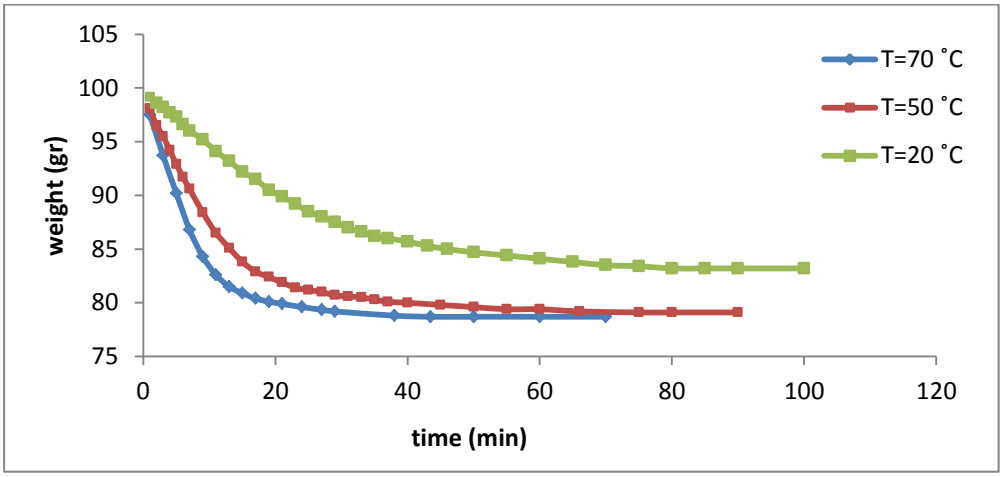

Figure 4-1: weight vs. time plots of 1-1.7 mm size under 90 lit/min for 100 gr of samples

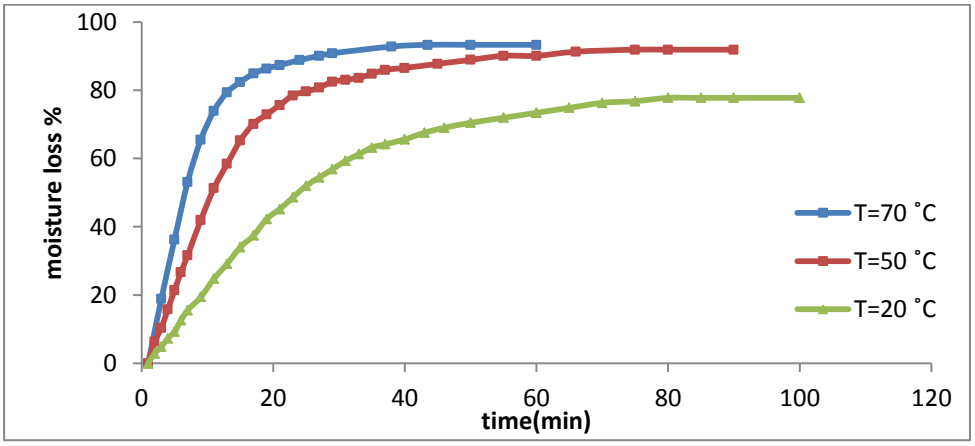

Figure 4-2: weight loss% vs. time plot for 1-1.7 mm size under 90 lit/min for 100 gr sample

As you can see in the graphs, there is a constant rate drying in the first stage followed by a falling rate drying. The constant rate drying corresponds to the removal of surface moisture of the particles which are poorly bound to the coal particle (water types of 4 and 5 in Allardic classification). When this moisture is removed a critical moisture content is left and the drying process enters the falling rate stage. The falling rate coresponds to the removal of the water inside the capilaries and pores of the particles (water type 3 of Allardic classification) which can be partially removed by physical treatments. This water has to diffuse to the surface to be removed by the air flow.

Figure 4-2 shows that air flow temperature directly affects the drying rate of coal particles in the constant rate stage. Comparing the results of 20 °C air inlet temperature, where no heat transfer occurs in bed, and the results of 70 °C, we can see that by increasing the drying temperature, moisture removal increases by around 40 % in the fisrt stage. In this stage higher air temperature increases evaporation rate and the particle surface temperature, resulting in higher moisture removal [29]. In the falling rate stage however, were interior water has to diffuse to the particle surface, temperature is not an effective parameter becasue the diffusion driving force is the concentration gradient from inside the particle towards the surface which is a function of particle moisture content and air moisture. Air moisture content is proven to be zero in all temperatures and thus, the falling rate stage is not affected by the temperature change significantly.

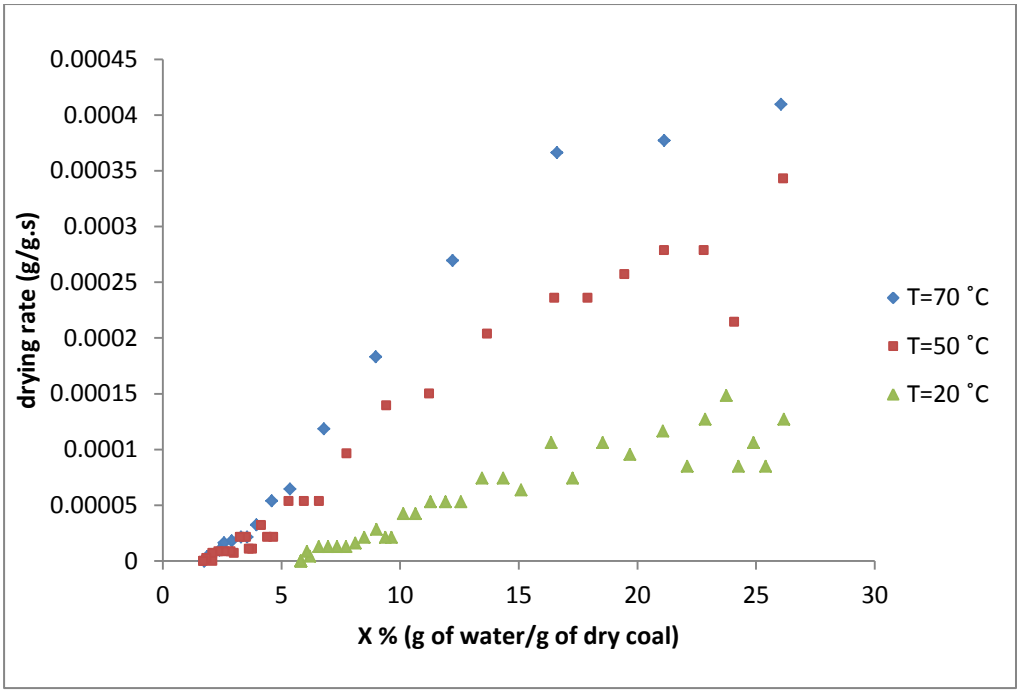

Figure 4-3: drying rate vs. X (gr water/gr dry coal)

Figure 4-3 shows the drying rate (g of removed water/g of dry coal per second) versus X (g of water/g of dry coal) for the same tests. It is obvious that by increasing the drying temperature from 20 °C to 70 °C, maximum drying rate (occurring in the constant rate period) is increased from around 0.00015 to 0.0004 [(g water)/(g dry coal).(s)] which is around 2.5 times faster.

4-1-2. Effect of gas inlet rate

To investigate the effect of gas inlet flow rate samples of 1-1.7 mm size with initial moisture of 21 % were tested under T_{air}=50 °C and different air flow rates. Air flow rates of 90 lit/min, 70 lit/min and 50 lit/min were applied to the samples.

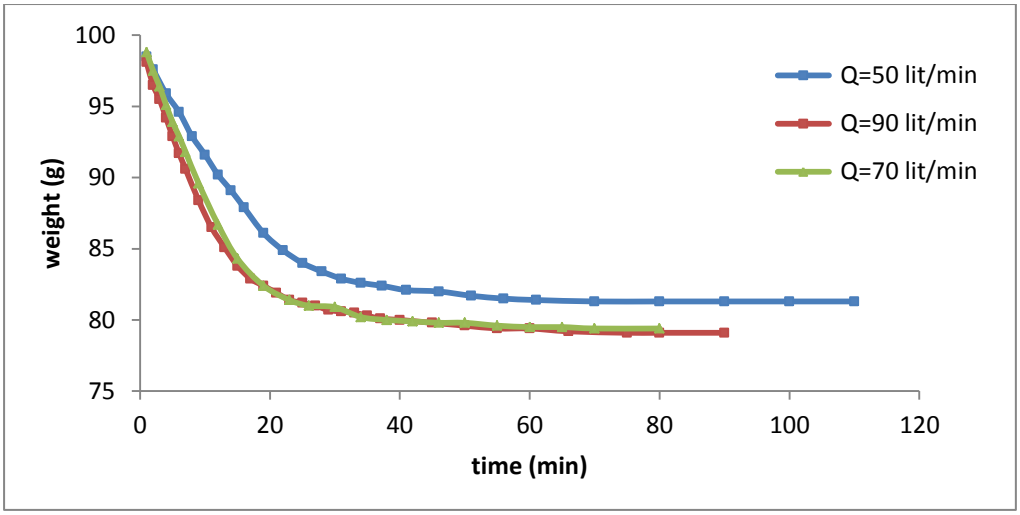

Figure 4-4: weight vs. time for 1-1,7 and T=50 ˚C at different air flow rates

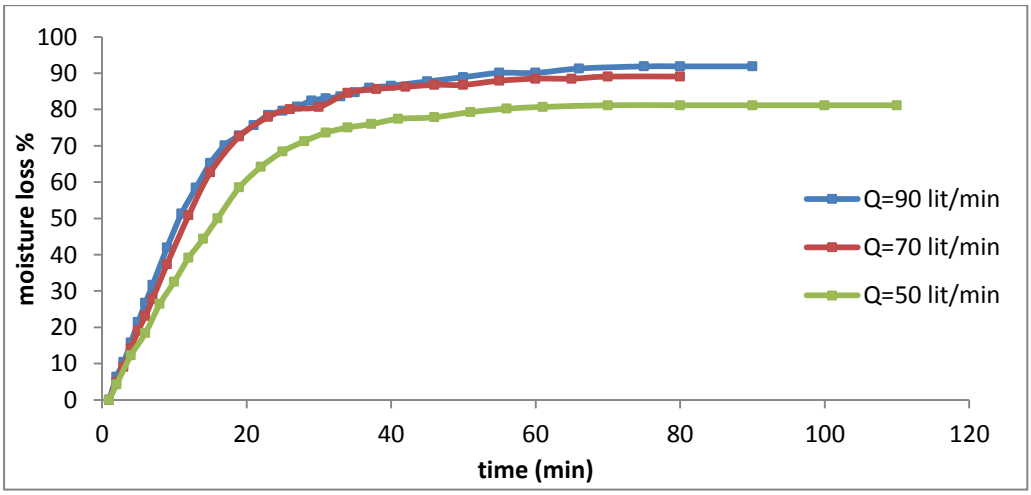

Figure 4-5: Moisture reduction % vs time for 1-1.7 mm size at 50 C under different air flow rate

As shown in figures 4-4 and 4-5 the air flow rate doesn't affect the drying of coal particles significantly. In 80 minutes of drying, the moisture reduction difference for the three flow rates is less than 6 %, suggesting the poor effect of air flow rate in the process. This is because coal particles, belonging to group D of Geldard classification, hardly show fluidization behavior. When the gas velocity corresponding to the minimum fluidization (calculated theoretically in Appendix A) is applied to the coal particles, we can hardly observe fluidization behavior and what can be seen is that particles mainly remain in a packed bed settlement due to low sphericity and high density. In

this condition, the upper particles receive more freedom and move slightly while except for some bubbles, not much movement happens inside the bed. In this situation, applying a gas flow rate to uniformly expand the bed and keep particle slightly separated from each other (the fluidization) is not possible. It can be concluded that if a bubbling and channeling bed is not desired, it is more economically efficient to keep the gas flow rate lower than the minimum fluidization velocity. In this study the term "fluidized bed" will be used only because tests were performed at the theoretical fluidization velocity. Figure 4-6 shows poor effect of gas flow rate in the bed.

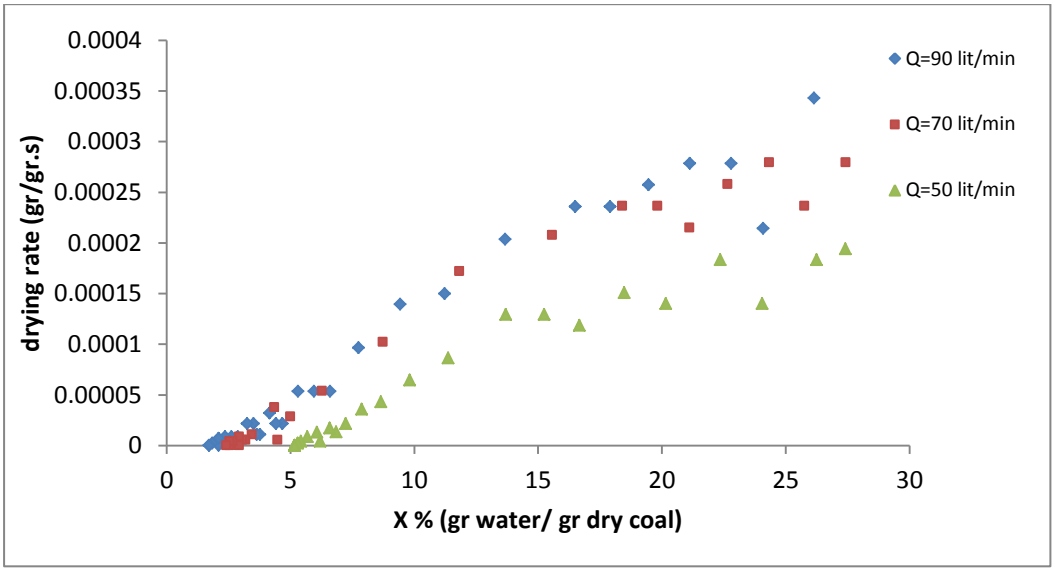

Figure 4-6: drying rate vs. X for 1-1.7 mm at 50 ˚C for different gas flow rates

4-1-3. Effect of particle size

To investigate the effect of particle size on the drying of lignite, two samples in the size range of 1-1.7 mm and 1.7-2.8 mm were dried in the fluidized bed under the same temperature and air velocity.

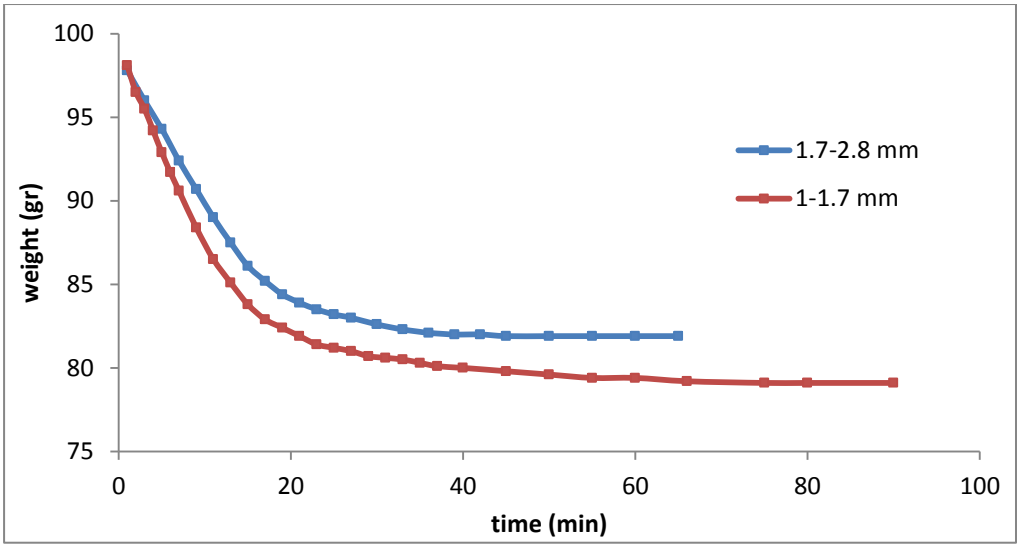

Figure 4-7: weight vs. time in T=50 ˚C and Q=90 lit/min

Weight loss vs time plot of the tests is presented in figure 4-7. As shown in the figure, the smaller size sample dries faster. Smaller particle means larger total surface area which leads to a higher heat and mass transfer. It is also accompanied by less thermal resistance and mass transfer resistance inside particles [29].

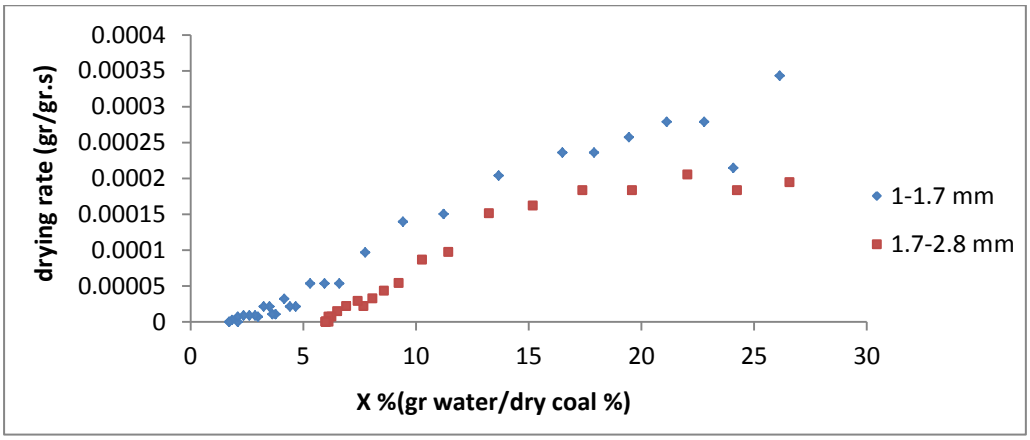

Figure 4-8: drying rate vs X % at T=50 °C and Q=90 lit/min

Figure 4-8 is a plot of the drying rate versus X and as expected, shows a lower final moisture content (equilibrium moisture content) for the smaller sized as well as a higher drying rate (around 50 % higher than coarse size).

4-2. Lignite drying using thermogravimetric method

Drying behavior of Canadian Lignite was tested in a Leco TGA701 thermogravimetric analyzer. Around 1 gram of samples in size, 1-1.7 mm size were dried for 10 hours under air with 50 °C and 70 °C temperatures and 7 ml/min flow rate.

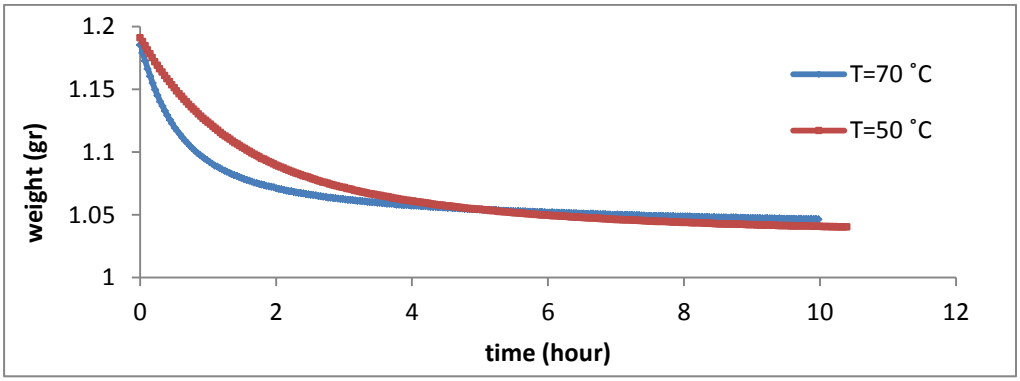

Figure 4-9: weight vs time curve for 1-1.7 mm

As expected figure 4-9 shows samples dried under 70 °C show a sharper weight loss during the constant rate period compared to sample dried under 50 °C air. In the falling rate period however, temperature is not affecting the drying rate significantly.

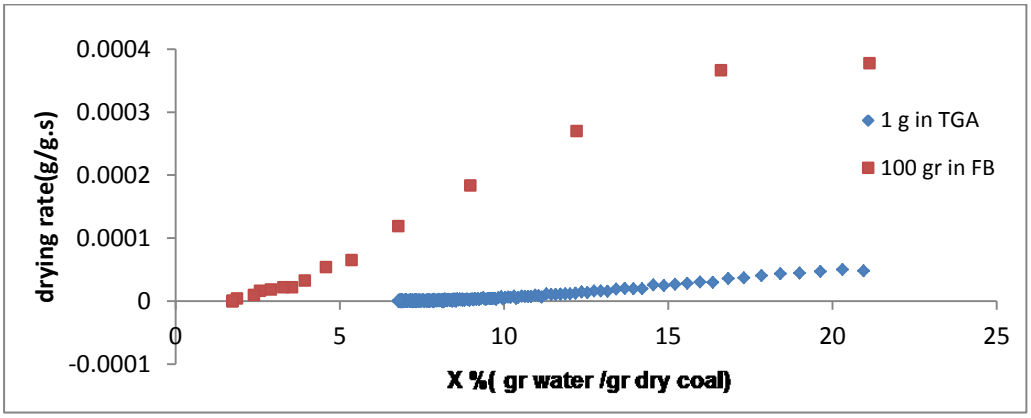

Figure 4-10: drying rate vs. X % at 70 C

Using figure 4-10 a comparison between the drying rate in a fluidized bed and in a TGA is possible. As expected the drying rate in a fluidized bed (due to high mass and heat transfer because of higher Reynolds Number) is much higher compared to a

drying condition where packed bed of particle are exposed to low air flow rates in chambers. The maximum drying rate in a fluidized bed is almost 10 times more which is due to high particle-air contact area leading to faster heat and mass transfer.

4-3. Mathematical modeling of drying of lignite in fluidized bed

Drying is a complex process comprising the heat and mass transfer between a particle and its surrounding and inside the particle. The movement of moisture from inside the particle towards the surface and from surface to the surrounding atmosphere depends on the structure and properties of the drying material, temperature and moisture concentration of the surrounding atmosphere and the amount and type of moisture in the particle [50].

Simulating this process provides information for assessment of energy and time conservation. Simulation is advantageous because real size experiments of a phenomenon can be time and energy consuming, expensive and even dangerous.

Mathematical models proposed in the literature include theoretical, semi-theoretical and empirical equations [50]. Theoretical models are derived from diffusion equation or simultaneous solving of mass and heat transfer. Semi-theoretical models are proposed based on Newton's cooling law which relates drying rate to the difference between moisture content at each time and the equilibrium moisture value of the sample [29]. Empirical models use the experimental data inclusively and suggest mathematical equations fitting the data.

In this chapter the drying data obtained from the experiment is curve fitted to some mathematical models introduced in the literature [29].

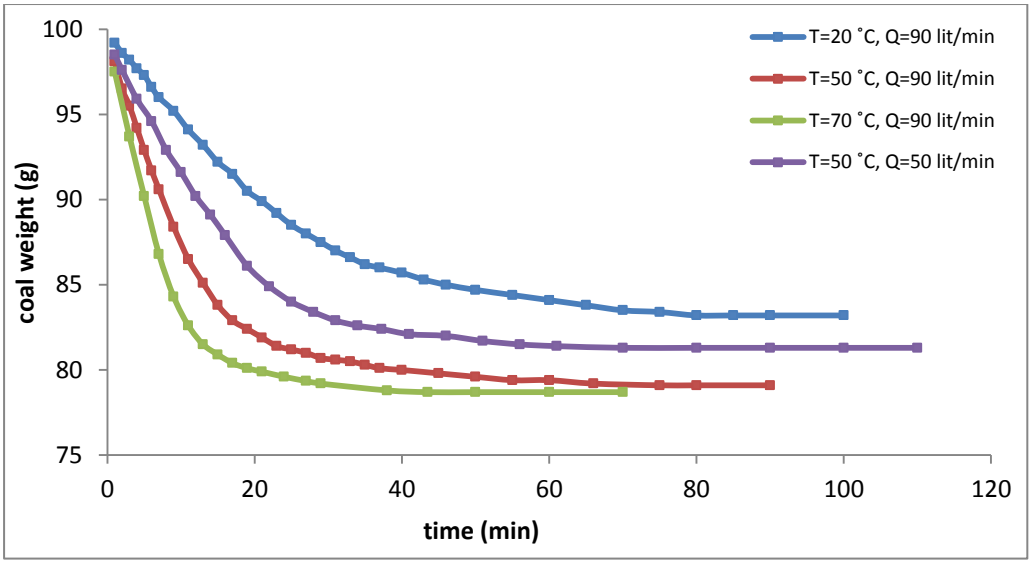

Figure 4-11: weight vs. time for different drying conditions of 1-1.7 mm size

Figure 4-11 presents the weight loss due to moisture removal vs. time for different drying conditions (temperature and air flow rates) of BD lignite. Drying starts with a constant rate and continues to a falling rate reaching zero rate at the end of each experiment. To find the best mathematical model which fits the process, 4 of the known models in the literature were used for curve fitting (table4-1).

Table 4-1: thin layer equations suggested in the literature [29]

Model name	Equation
Logarithmic	$X = a\ exp(-kt) + b$
Diffusion	$X = a\ exp(-kt) + (1-a)exp(-kbt)$
Simplified Fick	$X = a\ \exp(-c(t/L^2))$
Midilli-Kucuk	$X = a\ \exp\left(-k(t^n)\right) + bt$

The moisture data of sample (X=g water/g dry solid) at each time interval was plot vs. time and each of the models presented in the table 4-1 was curve fitted to the data. Regression was carried out using the commercially available data analyzer Matlab. The package uses the least square algorithm to iterate the analysis and adjust the parameters.

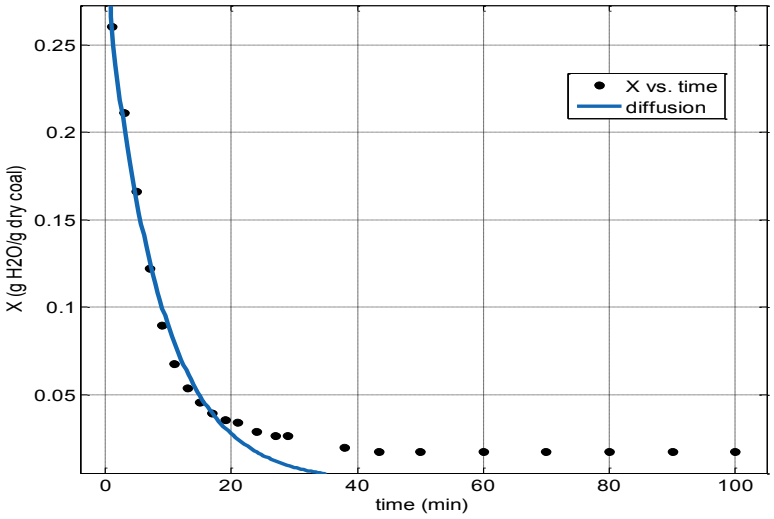

Figure 4-12: X vs. time for 1-1.7 mm dried in 70 C and 90 lit/min and diffusion fit

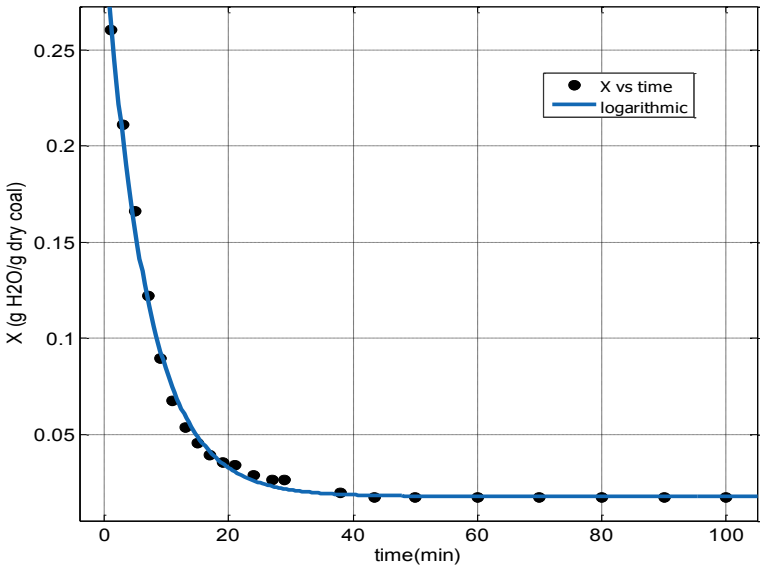

Figure 4-13: X vs. time for 1-1.7 mm dried in 70 C and 90 lit/min and logarithmic fit

Table 4-2: fitting equations and calculated coefficients for different drying conditions

Q(lit/min)	T(°C)	model	coefficients	R^2	SSE	RMSE
90	70	$X = a\ exp(-kt) + b$	a = 0.2903 k = 0.1486 b = 0.0179	0.996	0.000395	0.004559
90	70	$X = a\ exp(-kt) + (1 - a)exp(-kbt)$	a = 0.7111 b = 0.0220 k = 5.297	0.964 2	0.000352	0.01362
90	70	$X = a\ \exp(-c(t/L^2))$	a =0.2919 c = 0.222 L = 1.37	0.964 2	0.003527	0.01363
90	70	$X = a\ \exp(-k(t^n)) + bt$	a =3.14 k=0.1635 b=0.00024 n=0.9071	0.991 5	0.000833	0.006805
90	50	$X = a\ exp(-kt) + b$	a=0.2744 b=0.0192 k=0.09586	0.997 5	0.000460	0.003917
90	50	$X = a\ exp(-kt) + (1 - a)exp(-kbt)$	a=0.7241 b=0.01495 k=4.937	0.975 5	0.004313	0.003984
90	50	$X = a\ \exp(-c(t/L^2))$	a = 0.2778 b = 0.2912 c = 1.978	0.976 9	0.004334	0.01201
90	50	$X = a\ \exp(-k(t^n)) + bt$	a = 0.2993 b = 0.0002 k = 0.1082 n = 0.9118	0.995 1	0.000917	0.005625
90	20	$X = a\ exp(-kt) + b$	a = 0.2171 k =0.04059 b =0.06435	0.996 9	0.000534	0.003852
90	20	$X = a\ exp(-kt) + (1 - a)exp(-kbt)$	a = 0.7517 b=0.00497 k = 3.58	0.913 8	0.01464	0.02017
90	20	$X = a\ \exp(-c(t/L^2))$	a = 0.2514 b = 0.1163 c = 2.528	0.911 7	0.01499	0.02041
90	20	$X = a\ \exp(-k(t^n)) + bt$	a=0.277 b=0.00051 k=0.0306 n=0.9891	0.997 6	0.000414	0.003441

In table 4-2, RMSE stands for the root mean standard deviation, SSE is the sum of squares due to error and R-square is the coefficient of determination. Taking R-square as the main fit goodness parameter, the results of curve fitting shows that logarithmic model seems to be the best model to predict the drying behavior of lignite in the fluidized bed.

4-4. Calculating the mass transfer rate k_c

Drying materials in large scale is possible when a prior complete analysis of the process is available. Physical and thermal properties of the material to be dried, as well as heat and mass transfer conditions need to be studied. In case of drying in a fluidized bed, understanding the kinetic parameters is a crucial data required to design the drier. In this section the diffusion coefficient, mass transfer coefficient and the activation energy of lignite drying process is determined from the experimental data.

4-4-1. Diffusion coefficient

Mass diffusion is a type of mass transfer defined as "the movement of a fluid from an area of higher concentration to an area of lower concentration [51]." The general equation for the diffusion of the property momentum, heat or mass in the ζ direction is [52]:

$$\psi_\zeta = -\delta \frac{d\Gamma}{d\zeta} \tag{4-1}$$

Where:

- ψ_ζ is the flux of the property perpendicular to the area per unit of time
- δ is the diffusion coefficient (m^2/s)
- $d\Gamma/d\zeta$ is the driving force (concentration gradient in mass transfer, temperature difference in heat transfer…) per unit length

For diffusion mass transfer the above equation is expressed in the first Fick's law of diffusion as follows:

$$J_{A\zeta} = -D_{AB} \frac{dc_A}{d\zeta} \tag{4-2}$$

which determines the flux of the diffusion of Material A into B in the direction of ζ [52].

To calculate the diffusion coefficient for the fluidized bed the following series proposed by Crank [53] is used:

$$MR = \frac{M}{M_\circ} = \frac{8}{\pi^2}\sum_{n=1}^{\infty}\frac{1}{(2n-1)}\exp\left(-\frac{(2n-1)^2\pi^2 D_{AB}t}{4L^2}\right) \quad (4\text{-}3)$$

In this series the MR is the moisture ratio defined as the ratio of the moisture at each time divided by the initial moisture. M is the moisture content (gr water/gr dry coal) and $M_\circ$ is the initial moisture content, and L is the thickness which is the particle radius (r_p) in this study.

The first term of the above equation is used for a long drying time [39]. Hence:

$$MR = \frac{8}{\pi^2}\exp\left(\frac{\pi^2 D_{AB}t}{4L^2}\right) \quad (4\text{-}4)$$

Taking the Ln of both sides gives:

$$Ln(MR) = Ln\left(\frac{8}{\pi^2}\right) + \frac{\pi^2 D_{AB}}{4L^2}t = a + bt \quad (4\text{-}5)$$

Plotting Ln (MR) vs. time will give the slop of b. We can write:

$$D_{AB} = \frac{4L^2 b}{\pi^2} \quad (4\text{-}6)$$

The above equation along with the experimental data can be used to calculate the diffusion coefficient of lignite particles drying in the fluidized bed.

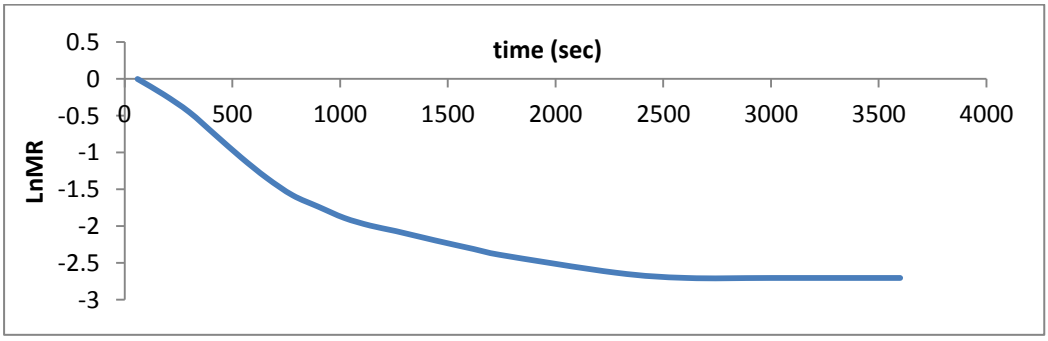

Figure 4-14: plot of ln MR vs time for d_p=1-1.7, T=70 °C, Q=90 lit/min,

Figure 4-14 shows the plot of Ln (MR) vs time for a particle size range of 1-1.7 mm, in 90 lit/min air flow of 70 °C.

Observing the plot we can see that the curve does not show one linear slope as expected. Thus we can include that the diffusion coefficient does not remain constant during the drying and as the particles moisture content reduces, the diffusion is also decreased.

As discussed in the previous section, in the first 900 seconds of drying, when the surface moisture is high enough to maintain drying at a constant rate there is a higher diffusion coefficient (constant rate drying period). As particles loose surface moisture, the water content inside the capillaries and micro pores need to be diffused to the surface by overcoming the resistance. This leads to a reduction in the moisture removal rate and a reduced diffusion coefficient (falling rate period).

The first and second stages of the process are presented in figures 4-15 and 4-16 with the linear lines fitted to the data.

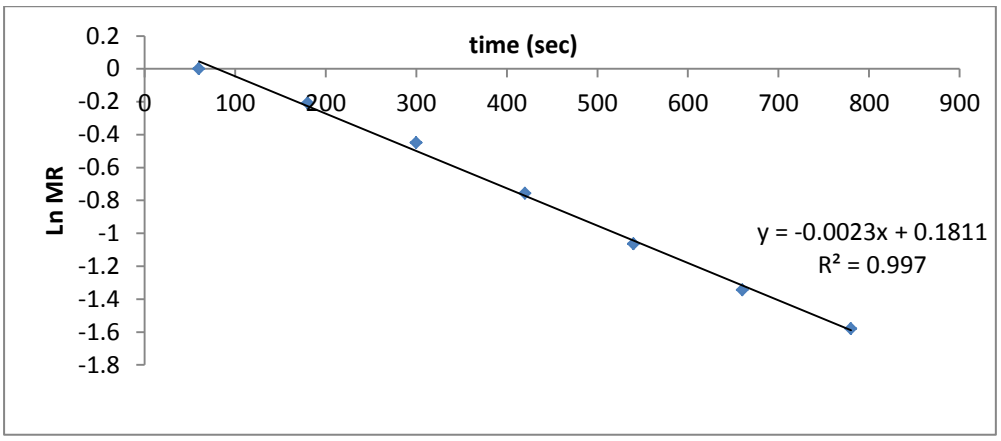

Figure 4-15: Ln MR vs. time for t=0-900 sec, T=70 ˚C , Q=90 lit/min

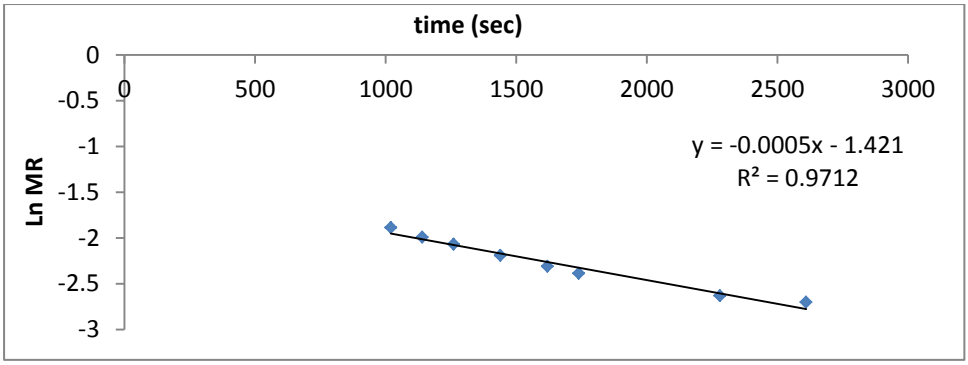

Figure 4-16: Ln MR vs. time fort=900-1750 sec, T=70 ˚C, Q=90 lit/min

As shown in the figures, the slope of the graph in the first stage is 2.3e-03 and for the second stage is 0.5e-03. The corresponding diffusion coefficient of the two stages will be 3.98e-10 m^2/s and 0.85e-10 m^2/s. The diffusion coefficient of other drying conditions is presented in table 4-3. Calculated values are in good agreement with data in the literature [29].

Table 4-3: diffusion coefficient for different drying conditions

d_p(mm)	T(˚C)	Q(lit/min)	b_1	D_1(m/s)	b_2	D_2(m/s)
1-1.7	70	90	2.3e-03	3.98-10	0.5e-03	0.85-10
1-1.7	50	90	1.2e-03	2.05-10	0.3e-03	0.51e-10
1-1.7	20	90	0.5e-03	0.85e-10	0.2e-03	0.34e-10
1-1.7	50	70	1.2e-03	2.05e-10	0.2e-03	0.34e-10

4-4-2. Mass transfer coefficient

For the Reynolds number in the range of 10-10000, for gases in a packed bed the correlation for mass transfer is as follows [52]:

$$J_D = \frac{0.4548}{\varepsilon} Re^{-0.4069} \qquad (4\text{-}7)$$

where J_D is dimensionless mass transfer factor. Using the void fraction and Reynolds number values, mass flux can be calculated from the above equation. We can write:

$$J_D = \frac{k_c}{u}(N_{Sc})^{\frac{2}{3}} \quad (4\text{-}8)$$

Which gives us the mass transfer coefficient k_c in (m/s) where u is the gas inlet velocity in (m/s) and N_{Sc} is the Schmidt number defined as:

$$N_{Sc} = \frac{viscous\ diffusion\ rate}{molecular\ diffusion\ rate} = \frac{\mu}{\rho D_{AB}} \quad (4\text{-}9)$$

Using the diffusion coefficient obtained from the previous section mass transfer coefficient of each run can be calculated. Table 4-4 shows the result for different drying conditions.

Table 4-4: mass transfer coefficients for different drying conditions

d_p(m)	T(°C)	Q(lit/min)	Re	J_D	D_1(m^2/s)	N_{Sc_1}	k_{c1}(m/s)	D_2	N_{Sc_2}	k_{c2} (m/s)
1-1.7	70	90	25.28	0.27	3.98e-10	51.67e03	7.8E-05	0.85e-10	2.4e05	2.78e-05
1-1.7	50	90	25.28	0.27	2.05e-10	100.03e03	5.03E-05	0.51e-10	4.03e05	1.98e-05
1-1.7	20	90	25.28	0.27	0.85e-10	241.9e03	2.80E-05	0.34e-10	6.05e05	1.51e-05
1-1.7	50	70	18.96	0.30	2.05e-10	100.02e03	4.17E-05	0.34e-10	6.04e05	1.26 e-05

4-4-3. Mass flux

To calculate the total flux in a bed the external solid surface area of particles for mass transfer A_{ex} should be calculated. To do so, assuming the total volume of the bed in m^3 (including the particles and voids) is V we can write:

$$a = \frac{6(1-\varepsilon)}{d_p} \quad (4\text{-}10)$$

Where a is the surface area/total volume of bed with spherical particles (m^2/m^3).

$$A_{ex} = aV \tag{4-11}$$

Mass conservation equation can be written as:

$$N_A A_{ex} = Q(c_{A2} - c_{A1}) \tag{4-12}$$

In the above equations c_{A1} can be taken as zero (zero inlet air moisture amount). To calculate the mass transfer rate of the bed plot of weight (g) vs time (s) can be used.

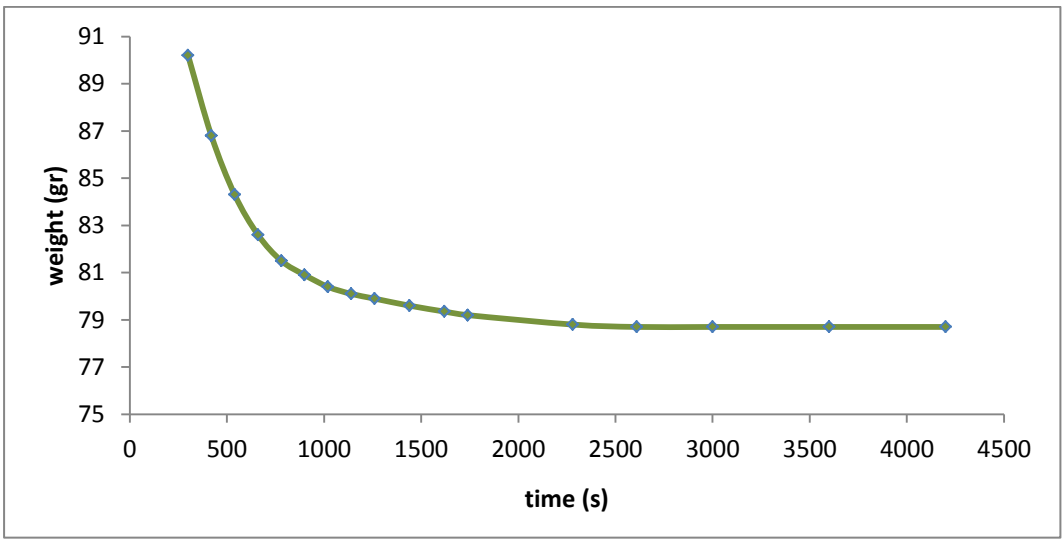

Figure 4-17: weight vs. time for T=70 °C, Q=90 lit/min and dp=1-1.7 mm

As we can see in figure 4-17 and discussed before, in the first 600 seconds a constant diffusion coefficient can be detected.

Calculating the slop of the weigh curve in the first 600 seconds we can write:

M_1=0.022 g/s. This is the amount of moisture released from the bed of coals in every second for the first 600 seconds in the outlet. This mass flow can be expressed as kg of water/ m^3 of air in the below equation:

$$c_{A2} = \frac{mass\ flow\ of\ water\ (\frac{g}{s})}{volume\ of\ air\ per\ second\ \left(\frac{m^3}{s}\right)} = \frac{0.022}{1.5 * 10^{-3}} = 14.66\ (\frac{g\ of\ H_2O}{m^3 of\ air})$$

For the external surface area we can write:

$$a = \frac{6(1-\varepsilon)}{d_p} = \frac{6 * 0.55}{0.0013} = 2538.46$$

$$A_{ex} = aV = 2538.46 * 0.0038 * 0.05 = 0.48\ m^2$$

And substituting in equation 20 we will have:

$$N_A = \frac{14.66 * 1.5 * 10^{-3}}{0.48} = 0.046\ {}^{g}/_{m^2.s}$$

Figure 4-18 shows a plot of weight vs time for different drying temperatures and the linear fitted curves. The slopes of the equation shown in the plot are used to calculate c_{A2} and N_A. Results of the calculation for 2 stages are presented in table 4-5.

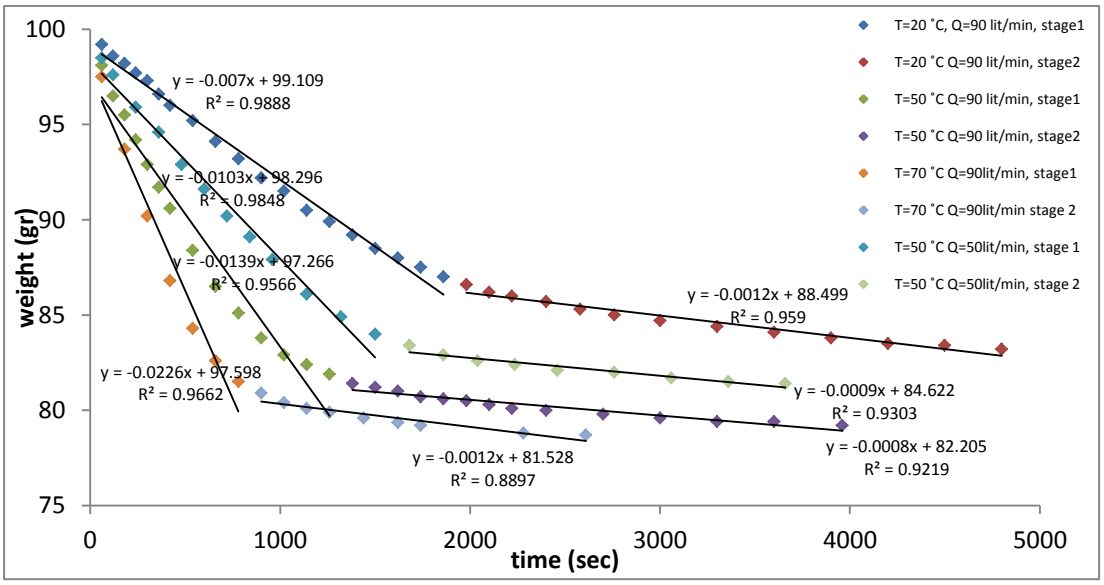

Figure 4-18: weight vs time for different drying conditions and fitted linear curves

Table 4-5: results of c_{A2} and N_A for different drying conditions

d_p(m)	T(°C)	Q(lit/min)	Re	A_{ex}(m)	c_{A2} stage1(g/m^3)	N_A stage1(g/m^2.s)	c_{A2} stage2(g/m^2.s)	N_A stage2(g/m^3)
1-1.7	70	90	25.28	0.48	14.66	0.046	0.8	0.0025
1-1.7	50	90	25.28	0.48	10	0.031	0.53	0.0016
1-1.7	20	90	25.28	0.48	4.26	0.013	0.8	0.0025
1-1.7	50	70	18.96	0.48	8.82	0.021	0.6	0.0014

4-4-4. Mass transfer coefficient using Stefan problem approach

The general mass transfer of species A can be expressed as:

Mass flow of species A per unit area=Mass flow of species A associated with bulk flow per unit area-Mass flow of species A associated with molecular diffusion per unit area

Or:

$$\dot{m}_A'' = Y_A(\dot{m}''_A + \dot{m}''_B) - \rho D_{AB}\frac{dY_A}{dx} \qquad (4\text{-}13)$$

Where:

$\dot{m}''_A$: mass flux of species A which is $\dot{m}_A/A$ (mass flow rate per unit area)

Y_A: mass fraction of species A

D_{AB}: binary diffusivity of water and air (m^2/s)

X: direction of mass transfer (m)

ρ: density (kg/m^3)

One of the simplest approaches to calculate the rate of moisture removal in the fluidized bed is the assumption of coal moisture to be free water contained in a column and exposed to air flow. Taking water vapor as species A and the air as species B we can write $\dot{m}''_B = 0$ (air is not diffusing in water vapor)

and thus the mass transfer rate equation becomes [54]:

$$\dot{m}_A'' = Y_A\dot{m}''_A - \rho D_{AB}\frac{dY_A}{dx} \qquad (4\text{-}14)$$

Saturation mass fraction of water:

$$Y_{water} = \frac{P_{sat}(T)}{P}.\frac{M_{water}}{M_{mix}} \qquad (4\text{-}15)$$

Where $P_{sat}(T)$ is the saturation pressure at the drying temperature, P is the atmosphere pressure, M_{water} is the molecular weight of water and M_{mix} is the interface mixture molecular weight.

Rearranging the equation and integrating will result in:

$$\dot{m}''_A = \frac{\rho D_{AB}}{L} \ln\left(\frac{1-Y\infty_{water}}{1-Y_{water}}\right) \quad (4\text{-}16)$$

To simplify the equation L=1 and we know $Y\infty_{water}=0$ (no moisture in the air).

Thus above equation becomes:

$$\dot{m}''_A = \rho D_{AB} \ln\left(\frac{1}{1-Y_{water}}\right) \quad (4\text{-}17)$$

Table 4-6: Mass flux of water leaving the bed calculated by Stefan approach

T(˚C)	P_{sat} (pa)	Y_{water}	$\dot{m}''_A$(g/m^2.s)
70	30866	0.22	7.40E-03
50	12210	0.079	2.25E-03
20	2310	0.0144	3.80E-04

Table 4-6 shows the mass flux values calculated using equation (4-17). Comparing the flux values in tables 4-5 and 4-6, it can be seen that the value of mass flux calculated by Stefan problem approach is significantly smaller than that of the experiments. However, we can apply the following correction to the mass transfer rate [55]:

$$\dot{m}''_A = \left[\rho D_{AB} \ln\left(\frac{1}{1-Y_{water}}\right)\right]\frac{Sh}{2} \quad (4\text{-}18)$$

Where Sh is the Sherwood number which can be calculated using Gunn correlation [56]:

$$Sh = Nu = (7 - 10\varepsilon + 5\varepsilon^2).\left(1 + 0.7Re^{1/5}Pr^{1/3}\right) + (1.33 - 2.4\varepsilon + 1.2\varepsilon^2)Re^{0.7}Pr^{1/3}$$

Where Re is calculated using equation (2-4) and Pr number value is 0.7 for air [57] . The calculated Sh number is 11.88 and the corrected mass transfer rates are presented in

Table 4-7: corrected Stefan values and experimental values for mas flux

T(˚C)	Corrected mass flux ($g/m^2.s$) $*10^3$	Experimental mass flux ($g/m^2.s$) $*10^3$
70	43.95	46
50	13.36	31
20	2.28	13

As table 4-7 shows, applying the Sherwood number correction improves the mass flux value for 70 ˚C drying significantly, but fails to result in an accurate value for lower drying temperatures.

4-5. Calculating the activation energy of drying

To calculate the activation energy of drying process of lignite, the drying rate k as a function of temperature can be expressed by Arrhenius equation as follows:

$$k = A\ exp(-E_a/RT) \tag{4-18}$$

Where k is the drying rate, A is the pre exponential factor, E_a is the activation energy, R is the universal gas constant (8.3143 kJ/mol) and T is the temperature in kelvin.

Value of k is calculated based on the first 10 minutes of drying which follows a constant rate in all temperatures for 1-1.7 mm sample and 90 lit/min gas flow rate. Values are presented in table 4-8.

Table 4-8: k and ln (k) values of each temperature for 1-1.7 mm size and 90 lit/min gas flow rate

Temperature (k)	Drying rate k (g/g.s)	Ln(k)
343	2.92E -04	-8.14
323	1.79E -04	-8.63
293	0.89E-04	-9.33

To obtain the E and A values, the natural logarithm of drying rate versus the reciprocal of temperature can be plot:

$$lnk = -(E_a/R)(1/T) + lnA \qquad (4\text{-}19)$$

Figure 4-9 is the plot of lnk vs. 1/T and the linear curve fitted gives the coefficients of equation 4-18.

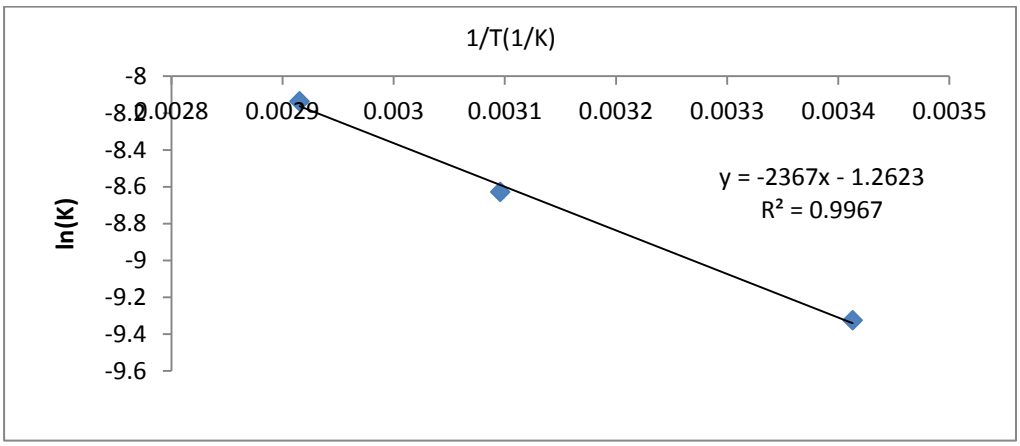

Figure 4-19: natural logarithmic plot of k vs. 1/T

The calculated activation energy and frequency factor are 19.68 kJ/mol and 0.283 s^{-1} respectively. These values are comparable with values reported in the literature [29].

The values of k can also be taken from the diffusion model (table 4-1) which proved to be the best fit for drying Canadian lignite. K values are presented in table 4-9.

Table 4-9: k values taken from diffusion curve fitted to the experimental results

T (˚C)	K	lnk
70	0.1486	-1.90
50	0.0959	-2.34
20	0.0406	-3.20

The corresponding activation energy and pre exponential factors are 21.78 kJ/mol and 312.82 s^{-1} respectively.

Comparing the results with the values of 21.17 kJ/mol and 0.877 s^{-1} from the literature [29], it can be concluded that the diffusion fit overpredicts the value of frequency factor but predicts the activation energy precisely.

Chapter 5: CFD modeling of lignite drying in a fluidized bed

5-1. Introduction

CFD modeling of fluidized beds is a challenging task due to the complex nature of the problem. The hydrodynamics and phase interaction of gas-solid flow are some of the problem complexities [49]. In this chapter, Ansys-Fluent 14.0 package has been used to simulate the drying of lignite particles in a fluidized bed. Despite the effort to model the drying process using the Arrhenius model (with the parameters calculated in section 4-5), only the constant rate drying period was successfully modeled in this study.

5-2. CFD Multiphase Models

In CFD analysis, two different approaches are available to model multiphase problems (i.e. gas-solid interaction in fluidized beds): the Euler-Lagrange approach and the Euler-Euler approach.

5-2-1. The Euler-Lagrange approach

In this approach the fluid phase is analyzed as a continuum and Navier-Stokes equations are solved for this phase. The dispersed phase is solved by tracing individual particles in the fluid field. The two phases exchange transport properties, i.e momentum etc. The main assumption made in this model is that the dispersed phase is occupying a low volume fraction in the system. This assumption makes this model appropriate to model spray dryers, and fuel combustion but poorly useful in modeling liquid-liquid mixtures, fluidized beds or generally systems with a large volume fraction of the dispersed phase [56][49] .

5-2-2. The Euler-Euler approach

In this approach both the fluid and the dispersed phases are treated as interpenetrating continua. Conservation equations are written for both phases and each phase's equations are related to the other using constitutive relations obtained from empirical information of the kinetic theory [56].

Fluent provides three different Euler-Euler models:

5-2-2-1.The VOF

The VOF is a surface tracking method suitable for immiscible fluids when the fluids interface position is to be studied. This model is applicable in problems such as free surface fluids [56].

5-2-2-2.The mixture

This model is designed for two or more phases of fluids or particulates. The model solves the mixture momentum equations, and using the relative velocities, solves for the dispersed phases. Sedimentation is a good example of application of this model [56].

5-2-2-3.The Eulerian

This is the most sophisticated model for multiphase analysis. It solves momentum and continuity equations for each phase and couples the results using pressure and exchange coefficients between the phases. Fluidized beds are solved using this method [56].

In this study, Eulerian model was used to simulate the fluidized bed dryer.

5-3. Equations for Eulerian model

Conservation of mass [56]:

$$\frac{1}{\rho_{rq}}\left(\frac{\partial}{\partial t}\left(\alpha_q \rho_q\right) + \nabla.\left(\alpha_q \rho_q \vec{v}_q\right) = \sum_{p=1}^{n}\left(\dot{m}_{pq} - \dot{m}_{qp}\right)\right) \qquad (5\text{-}1)$$

Conservation of energy [56]:

$$\frac{\partial}{\partial t}\left(\alpha_q \rho_q h_q\right) + \nabla.\left(\alpha_p \rho_p \vec{v}_q h_q\right) = -\alpha_q \frac{\partial p_q}{\partial t} + \tau_q : \nabla \vec{v}_q - \nabla . \vec{q}_q + S_q +$$

$$\sum_{p=1}^{n}(Q_{pg} + \dot{m}_{pq} h_{pq} - \dot{m}_{qp} h_{qp}) \qquad (5\text{-}2)$$

Fluid- Fluid Momentum balance for fluid phase q [56]:

$$\frac{\partial}{\partial t}\left(\alpha_q \rho_q \vec{v}_q\right) + \nabla.\left(\alpha_q \rho_q \vec{v}_q \vec{v}_q\right) = -\alpha_q \nabla p + \nabla . \tau_q + \alpha_q \rho_q \vec{g} +$$

$$\sum_{p=1}^{n}\left(K_{pq}\left(\vec{v}_p - \vec{v}_q\right) + \dot{m}_{pq}\vec{v}_{pq} - \dot{m}_{qp}\vec{v}_{qp}\right) + (F_q + F_{lift,q} + F_{vm,q}) \qquad (5\text{-}3)$$

Where τ_q is the stress-strain tensor [56]:

$$\tau_q = \alpha_q \mu_q\left(\nabla \vec{v}_q + \nabla \vec{v}_q^T\right) + \alpha_q\left(\lambda_q - \frac{2}{3}\mu_q\right)\nabla . \vec{v}_q I \qquad (5\text{-}4)$$

And K_{pq} is the interphase momentum exchange coefficient.

For solid- fluid momentum exchange an equation similar to (5-3) is used with K_{ls}, momentum exchange coefficient between fluid l and solid s. Fluent uses different models to define this momentum exchange coefficient. Some of the available models include Syamlal-Obrein, Gidaspow, Wen-Yu etc. The best model to predict the solid-gas exchange coefficient for fluidized beds is proved to be Syamlal-Obrein.

In this study, Syamlal-Obrein drag was used to evaluate the fluidization behavior.

5-4. Syamlal-O'brein Drag model

The general form for the solid-gas exchange coefficient is[56]:

$$K_{ls} = \frac{\alpha_s \rho_s f}{\tau_s} \qquad (5\text{-}5)$$

Where τ_s is the "particulate relaxation time" in the form of:

$$\tau_s = \frac{\rho_s d_p^2}{18\mu_l} \qquad (5\text{-}6)$$

and f includes a drag function C_D based on relative Reynolds number.

In the model suggested by Syamlal and Obrein (1987) C_D is defined as:

$$C_D = \left(0.63 + \frac{4.8}{\sqrt{\frac{Re_s}{v_{r,s}}}}\right)^2 \quad (5\text{-}7)$$

Where Re_s is defined as:

$$Re_s = \frac{\rho_l d_p(|\vec{v}_s - \vec{v}_g|)}{\mu_l} \quad (5\text{-}8)$$

And $v_{r,s}$ is the terminal velocity ratio:

$$v_{rs} = 0.5(A - 0.06Re_s + \sqrt{(0.06Re_s)^2 + 0.12Re_s(2B - A) + A^2}\ ) \text{ [58]} \quad (5\text{-}9)$$

With: $A = \alpha_g^{4.14}$ (5-10) and

$B = p\alpha_g^{1.28}$ (5-11) for $\alpha_g \leq 0.85$

And $B = \alpha_g^{q}$ (5-12) for $\alpha_g > 0.85$

The values of p and q are 0.8 and 2.56 respectively. Then the solid-fluid exchange coefficient becomes [58]:

$$K_{sl} = \frac{3\alpha_s\alpha_g\rho_g}{4v_{rs}^2 d_s} C_D\left(\frac{Re_s}{v_{rs}}\right)|\vec{v}_s - \vec{v}_g| \quad (5\text{-}13)$$

5-5. Boundary conditions

Inlet:

- Gas velocity = 0.4 m/s
- Gas temperature = 293K, 343 K
- Mass fraction of H_2O= 0

Outlet:

- outflow

Wall:

- Momentum: No slip
- Species: Zero diffusive flux

5-6. Initial conditions

- Solid volume fraction= 0.55
- Solid temperature= 300 K
- Solid velocity= 0

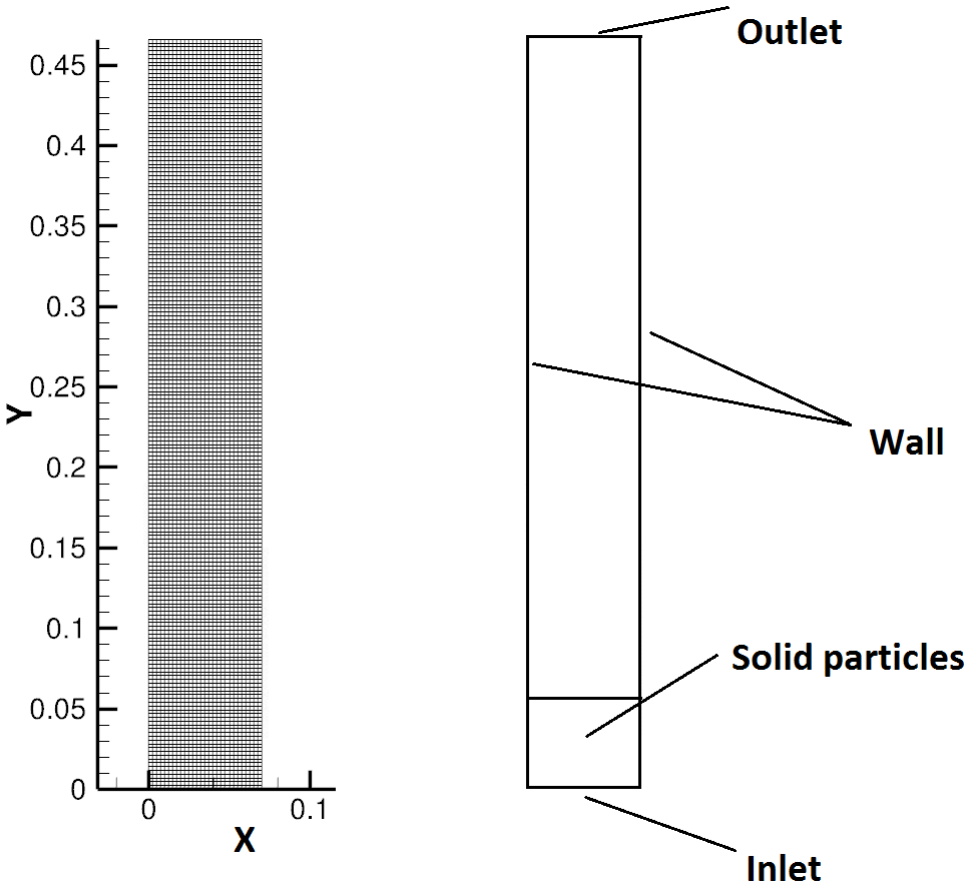

Figure 5-1: Bed mesh and Boundaries

This model was applied to the Fluent along with the input data and settings presented in tables 5-1 and 5-2.

Table 5-1: Input parameters for Fluent

Parameter	Value
Particle diameter	1.3e-03 m
Particle density	1400 kg/m^3
Solid volume fraction	0.55
Packing limit	0.58
Gas velocity	0.4 m/s
Gas temperature	20˚C and 70 ˚C
Solid initial temperature	20 ˚C (293 K)
Mass transfer rate	0.06 and 0.21 kg/m^3.s
Time steps	10e-04 s
No. of iteration per time step	70
Operating pressure	101325 pa
Number of mesh cells	5544
Min/Max cell size	2.35e-03/2.493-03 m^2
Mesh aspect ratio	1.45
Smallest Residual	10e-04

Table 5-2: Solver Spatial discretization

Parameter	Spatial Discretization
Gradient	Least square cell based
Momentum	Quick
Volume fraction	Modified HRIC
Energy	Quick
Gas species	Quick
Solid species	Quick

In table 5-1, the value for mass transfer rate is the experimental values for 70 ˚C and 20 ˚C tests. The model predicts minimum fluidization velocity of 30.66 m/s for the bed which is 25% less than 0.4 m/s. This model was used to model the bed momentum exchange and the results for solid volume fraction are shown in figure 5-2.

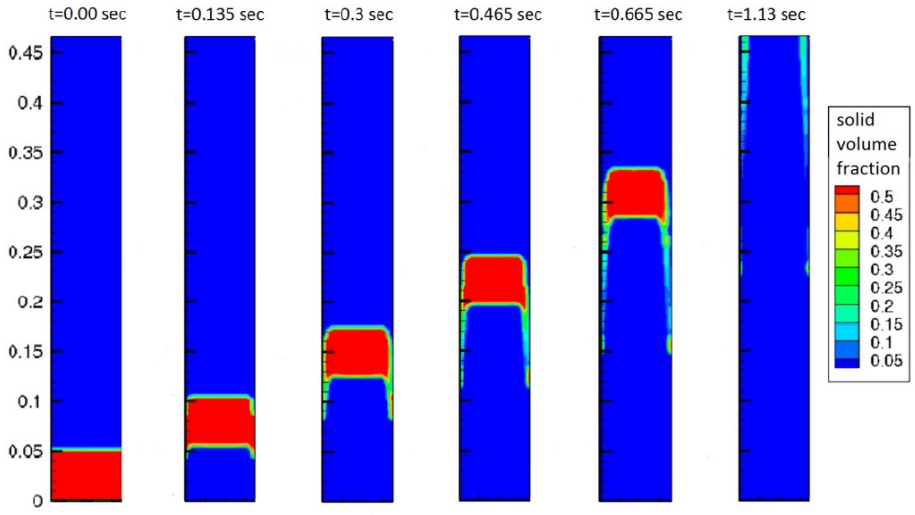

Figure 5-2: solid volume fraction in the first 1.13 sec using Syamlal-Obrein Drag model

As you can see in figure 5-2, the solid phase leaves the bed in the first 1.13 sec entirely, proving that the drag model does not predict the bed behavior correctly.

5-4. Tuned Syamlal-Obrein model

To make Syamlal-Obrein drag model predict the bed momentum exchange correctly, p and q coefficients need to be tuned to predict the appropriate velocity. To do so, we need to know the value for the particle terminal velocity ratio. We can write:

$$v_{r,s} = \frac{Re_s}{Ar^*} \tag{5-14}$$

Where Re_s can be calculated from equation (5-8) and Ar^* is a dimensionless function of the Archimedes number as:

$$Ar^* = \left(\frac{\sqrt{4.8^2 + 2.52\left(\sqrt{\frac{4Ar}{3}}\right)} - 4.8}{1.26} \right)^2 \tag{5-15}$$

Substituting the value for $v_{r,s}$ as 0.164, (which can be compared to 0.277, the value calculated by default p and q numbers) in equation 5-9 and iterating for A and B (using a programming code) the calculated values of coefficients p and q for this case were 0.491 and 5.66223 respectively. These values were used in a UDF file which is compiled by fluent to evaluate the solid-gas momentum exchange coefficient using Syamlal-Obrein model. Figure 5-3 shows the solid volume fraction during the first 5.22 sec of the modeling using the tuned drag model. It can be noticed that the bed reached a stable condition in 0.5 sec.

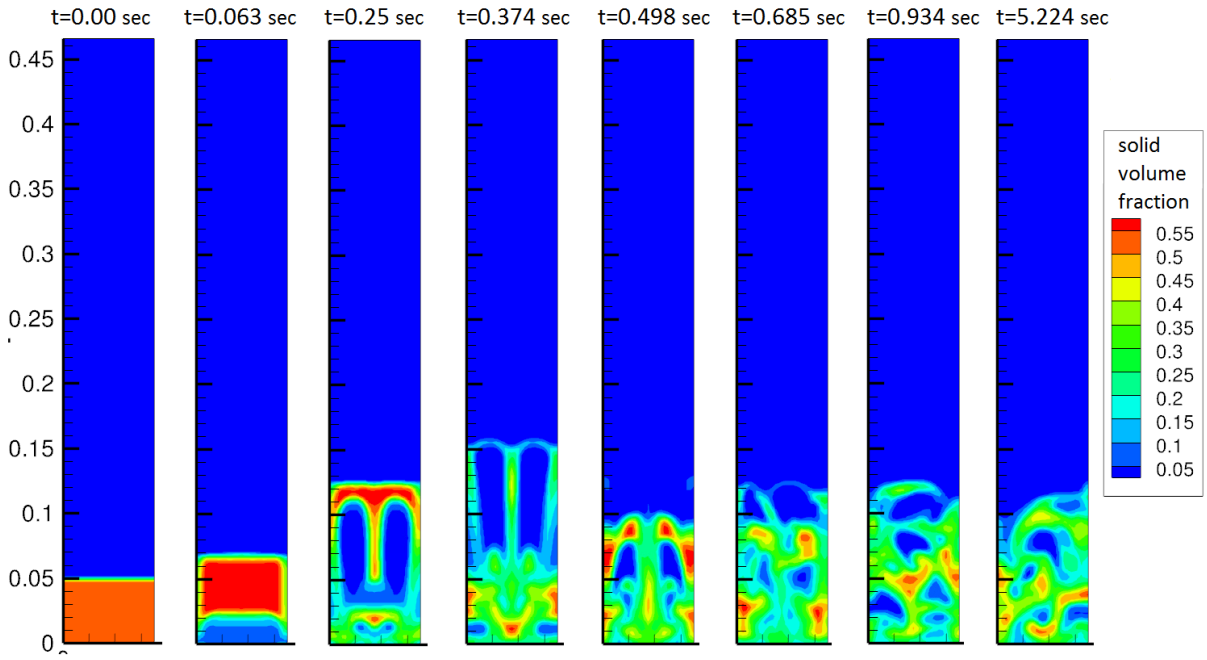

Figure 5-3: solid volume fraction calculated by tuned Syamlal-Obrein drag model

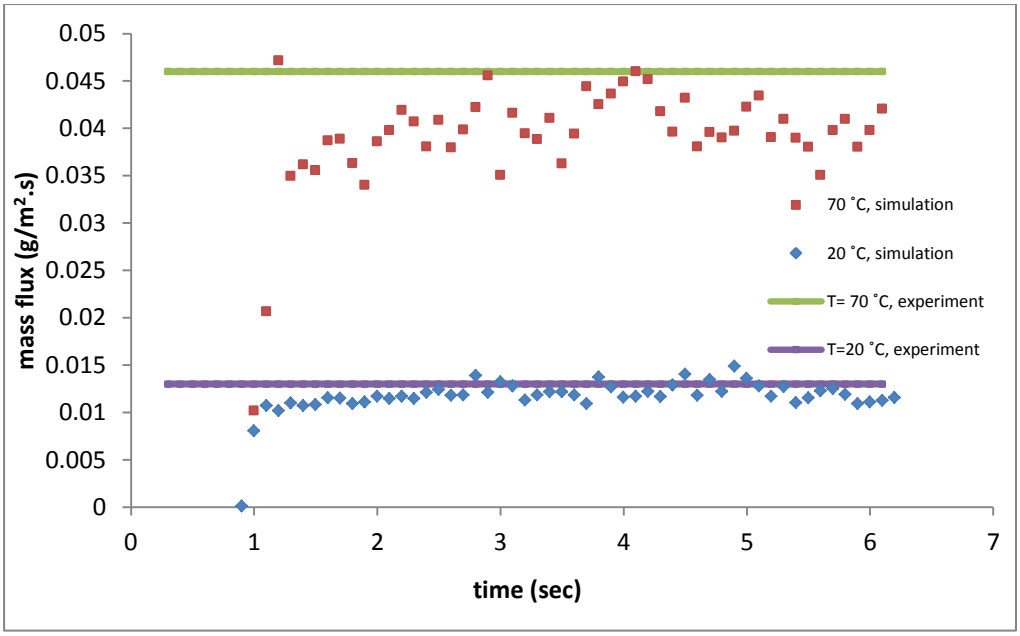

Figure 5-4: mass flux vs. time of H2O at the outlet for T=20 ˚C and 70 ˚C

Figure 5-4 shows a plot of mass flux of water versus time for 2 different drying temperatures. The plot shows that the water flux for 70 ˚C is almost 5 times higher than that of 20 ˚C. Comparing the software results with that of the experiment (table 4-5), it can be seen that the software has predicted the moisture removal successfully.

Chapter 6: Spontaneous combustion of lignite

To evaluate the spontaneous combustion risk of dried lignite, a series of experiments in a TGA-DSC were carried out. Around 10 mg of dried samples were heated up in the TGA-DSC in air atmosphere. Samples were heated up from room to 400 °C at different heating rates of 0.4 °C/min, 1 °C/min and 2 °C/min. Sample was then kept in an isotherm condition for 1 hour before cooling down to room temperature. The weight loss and heat flow of the samples were recorded by the instrument.

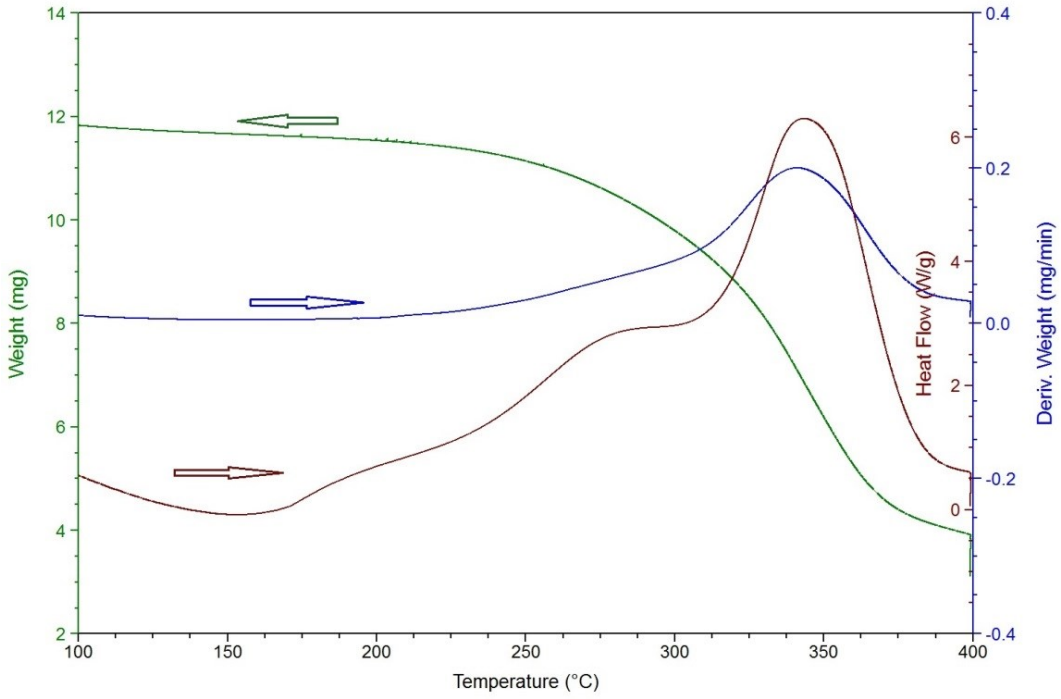

Figure 6-1: TGA-DSC signal of 2 C/min test

Figure 6-1 is the plot of weight, weight derivative and heat flow versus temperature for the 1 °C/min run. As you can see in the plot, the peaks indicate a reaction in the sample at a certain temperature. In the heat flow curve, the highest peak corresponds to the combustion of coal sample. In this

study, the onset temperature of the curves, were the sample starts releasing heat is taken as the temperature of spontaneous reaction.

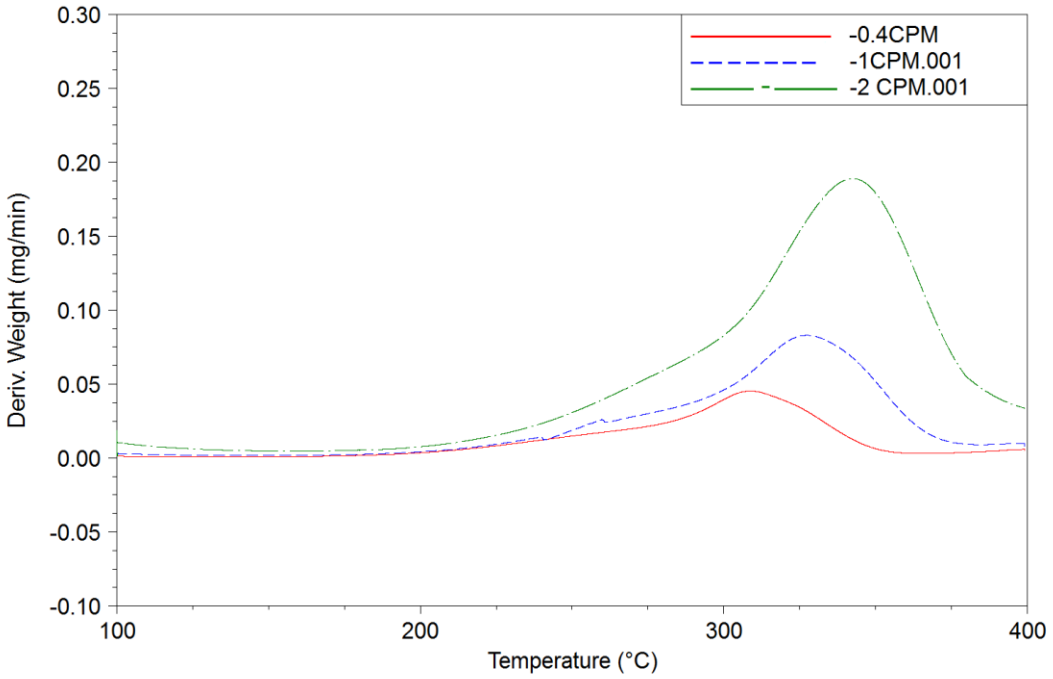

Figure 6-2: weight loss derivative of dried samples at 0.4, 1, 2 °C/min

Figure 6-2 is a plot of the weight derivative vs. temperature for the three runs. As expected, in higher heating rates, the reaction happens in a higher temperature which is due to a thermal lag.

To study the spontaneous combustion kinetics, the Semenov theory was used. According to this theory, the difference between the heat production and heat loss of the system defines the risk of an explosion in the system. Writing the energy balance in this way we can have [47]:

$$C_p M_0 \frac{dT}{dt} = \Delta H M_0 \, A exp(-\frac{E_a}{RT}) - US(T - T_0) \qquad (6\text{-}1)$$

Where:

C_p is the heat capacity of the system

M_0 is the initial mass of the reactant

ΔH is the heat of combustion per unit mass of reactant

A is the pre exponential factor

E_a is the activation energy

U is the overall heat transfer rate

S is the total surface area

T_0 is the ambient temperature

At the critical temperature both dT/dt and d(dT/dt)/dT are equal to zero and the ambient temperature must be equal to the self-heating oxidation (SHOT) [47]. So we will have:

$$\Delta HAM_0 \exp\left(-\frac{E_a}{RT_{cr}}\right) = US(T_{cr} - T_0) \quad (6\text{-}2)$$

And

$$\frac{\Delta HAM_0 E_a}{RT_{cr}^2} \exp\left(-\frac{E_a}{RT_{cr}}\right) = US \quad (6\text{-}3)$$

Dividing the two equations and rearranging for T_0 will give:

$$T_0 = SHOT = T_{cr} - \frac{RT_{cr}^2}{E_a} \quad (6\text{-}4)$$

To be able to calculate SHOT, activation energy, heat of combustion and pre-exponential factor can be calculated using the TGA-DSC data.

The same calculations that were carried out for activation energy of drying can be used to calculate spontaneous combustion activation energy. This included plotting LnK vs. 1/T for the reaction and taking a linear regression. In here the reaction rate and T data of different heating rate runs were used at 50 % of conversion.

Table 6-1: kinetic values of combustion in different heating rates

T (˚C)	Heating rate (˚C/min)	Reaction rate (mg/min)	ln Rate
259.18	0.4	0.034	-3.372
315.23	1	0.069	-2.662
333.06	2	0.18	-1.682

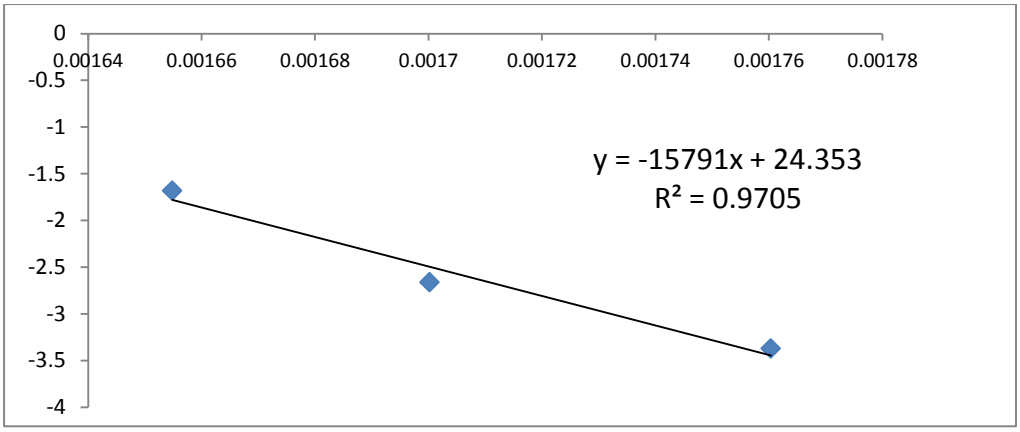

Figure 6-3: ln rate vs. 1/T at conversion of 0.5

As figure 6-3 shows, linear regression of the data gives the activation energy of 131.29 kj/mol and pre-exponential factor of 3.77e10 1/s.

Table 6-2: thermodynamic and kinetic of dried coal

Heating rate (°C/min)	ΔH (J/kg)	M_0 (mg)	S (mm^2)	T_{onset}(°C)	T_{cr} (°C)	SHOT(°C)
0.4	8785	13.47	580.347	148	154.5	142.9265
1	14458	10.5	452.386	160	164	151.9064
2	15243	12.96	558.374	178.3	176	163.2331

Table 6-2 presents the SHOT calculated values. As you can see SHOT values are good estimation of the onset temperature at which coal particles start releasing heat, leading to the spontaneous combustion.

Chapter 7: Summary and Conclusion

7-1. Summary

- Low temperature coal drying was studied in a pilot scale fluidized bed dryer. Lignite samples in the size range of 1-2.8 mm, with initial moisture of 21% were dried in the temperature range of 20 ˚C to 70 ˚C.
- Samples density was measured to be 1400 kg/m3 using the water displacement method.
- Fluidization regime was not effectively achieved in the bed because lignite samples, belonging to the group D of Geldard classification (known to be difficult to be fluidized) have high density, large particle size and low sphericity.
- Temperature showed a great effect on the drying rate in the constant rate period while being poorly effective in the falling rate period.
- Decreasing gas flow rate to 30 % below the theoretical minimum fluidization velocity showed satisfactory drying results.
- Modeling the lignite drying as a packed bed of free water exposed to low air stream under predicted the drying rate. Because despite the fact that particles are not fluidized in the bed, the upward air velocity through particles provides a high mass and heat transfer.
- Increasing particle size decreased the mass transfer rate and coefficient due to thermal lag and a smaller surface area contact.
- Drying data was curve fitted using mathematical models available in the literature and the logarithmic model best fitted the drying of lignite.

- Diffusion coefficient of lignite drying was calculated using the experiment data and was in a good degree of agreement with the value reported in the literature.
- Fluidized bed dryer was modeled using CFD analysis. Default Syamlal-Obrein drag model failed to predict the velocity profile correctly but tuning the model's coefficients improved the accuracy of the model compared to the experiment. Constant rate drying was successfully modeled in Fluent using a single mass transfer mechanism.
- Spontaneous combustion kinetic of dried lignite was studied. The onset temperature of the mass derivative curve, corresponding to the spontaneous combustion was measured experimentally and using the Semenov theory the temperature was calculated and showed good agreement with the measured value.

7-2. Conclusion

- Based on the data analysis, when drying lignite coal particles in a packed bed dryer, it is more efficient to use higher drying temperatures in the constant drying period and lower drying temperatures in the falling rate period.
- If spouted bed is not desired to be used for lignite drying, packed bed of lignite particles can be dried efficiently without increasing air velocity to the theoretical minimum fluidization.
- The self-heating oxidation temperature of lignite can be calculated using the Semenov theory. This temperature can be calculated and used to predict the reaction temperature.

Reference

[1] "world coal association" http://www.worldcoal.org. [Accessed: 20-Oct-2014].

[2] "Energy industry today" http://www.energy.einnews.com. [Accessed: 22-Sep-2014].

[3] J. Yu, A. Tahmasebi, Y. Han, F. Yin, and X. Li, "A review on water in low rank coals: The existence, interaction with coal structure and effects on coal utilization," *Fuel Process. Technol.*, vol. 106, pp. 9–20, Feb. 2013.

[4] coal association of Canada, "careers in coal." http://www.careersincoal.ca/mine-map/.

[5] "Alberta energy" http://www.energy.alberta.ca

[6] R. S. D.J. Allardice, L.M. Clemow, G. Favas, W.R. Jackson, M. Marshall, "The characterisation of different forms of water in low rank coals and some hydrothermally dried products," *Fuel*, vol. 82, pp. 661–667, 2003.

[7] J. Choung, C. Mak, Z. Xu, "Fine coal beneficiation using an air dense medium," *coal Prep.*, pp. 1–15, 2006.

[8] R. G. Domazetis, P. Barilla, B.D. James, "Treatments of low rank coals for improved power generation and reduction in greenhouse gas emissions," *Fuel Process. Technol.*, vol. 89, pp. 68–76, 2008.

[9] P. C. Dave, "Dry Cleaning of Coal by a Laboratory Continuous Air Dense Medium Fluidized Bed Separator", MSc thesis, Mining Engineering, University of Alberta, 2012.

[10] H. Katalambula and R. Gupta, "Low-Grade Coals : A Review of Some Prospective Upgrading Technologies," *Energy and Fuels*, vol 23, pp. 3392–3405, 2009.

[11] C.E. Salmas, A.H. Tsetsekou, K.S. Hatzilyberis, G.P. Androutsopoulos, "Evolution lignite mesopore structure during drying. effect of temperature and heating time," *Dry. Technol.*, vol. 19, pp. 35–64, 2001.

[12] N. Sarunac, E. K. Levy, M. Ness, C. W. Bullinger, J. P. Mathews, and P. M. Halleck, "A Novel Fluidized Bed Drying and Density Segregation Process for Upgrading Low-Rank Coals," *Int. J. Coal Prep. Util*, vol. 29, no. 6, pp. 317–332, Dec. 2009.

[13] I.J. Lynch, D.S. Webster, “Effect of thermal treatment on the interaction of brown coal and water: a nuclear magnetic resonance study,” *Fuel*, vol. 61, pp. 271–275, 1982.

[14] S.C. Mraw, D.F. Naas-O'Rourke, “Water in coal pores: low-temperature heat capacity behavior of the moisture in Wyodak coal,” *Science*, vol. 205, pp. 901–902, 1979.

[15] D.J. Allardice, D.G. Evans, "Analytical Methods for Coal and Coal Products″. New York: Academic Press, 1978.

[16] W. G. Willson, D. Walsh, and W. (Bill)Irwinc, “Overview of Low-Rank Coal (LRC) Drying,” *Coal Prep.*, vol. 18, no. 1–2, pp. 1–15, Jan. 1997.

[17] M. Karthikeyan, W. Zhonghua, and A. S. Mujumdar, “Low-Rank Coal Drying Technologies—Current Status and New Developments,” *Dry. Technol.*, vol. 27, no. 3, pp. 403–415, Feb. 2009.

[18] P. K. Chen, Z., Wu, W., Agarwal, “Steam-drying of coal. Part 1. Modeling the behavior of a single particle,” *Fuel*, vol. 79, pp. 961–973, 2000.

[19] “ http://www.wikipedia.com" [Accessed: 22-Oct-2014].

[20] Bergins, Christian, “Science and Technology of the Mechanical / Thermal Dewatering,” 2005.

[21] GEA group, “GEA Process Engineering Inc.” http://www.niroinc.com. [Accessed: 22-Oct-2014].

[22] C. Mak, “Fine coal cleaning using an air dense medium fluidized bed,” Alberta, 2007.

[23] M. Rhodes, “Introduction to particle technology,” 2nd ed., M. Rhodes, Ed. pp. 193–235.

[24] P. Zhao, Y. Zhao, Z. Luo, Z. Chen, C. Duan, and S. Song, “Effect of operating conditions on drying of Chinese lignite in a vibration fluidized bed,” *Fuel Process. Technol.*, vol. 128, pp. 257–264, Dec. 2014.

[25] G. Chase, “Solids notes,” 2004, pp. 5–1 to 5–11.

[26] D. Geldart, “Types of Gas Fhidization,” *Powder Technol.*, vol. 7, pp. 285–292, 1973.

[27] W.-C. Wang, “Laboratory investigation of drying process of Illinois coals,” *Powder Technol.*, vol. 225, pp. 72–85, Jul. 2012.

[28] K. S. Vorres, “Effect of Temperature, Sample Size, and Gas Flow Rate on Drying on Beulah-Zap Lignite and Wyodak Subbituminous Coal,” *Energy & Fuels*, vol. 8, no. 2, pp. 320–323, Mar. 1994.

[29] A. Tahmasebi, J. Yu, Y. Han, H. Zhao, and S. Bhattacharya, “Thermogravimetric study and modeling for the drying of a Chinese lignite,” *ASIA-PACIFIC J. Chem. Eng.*, vol. 8, no. February, pp. 793–803, 2013.

[30] H. Wang, “Kinetic Analysis of Dehydration of a Bituminous Coal Using the TGA Technique,” no. 10, pp. 3070–3075, 2007.

[31] C.Srinivasakannan and N.Balasubramanian, “A simplified approach to the drying of solids in a batch fluidized bed,” *Brazilian J. Chem. Eng.*, vol. 19, pp. 293–298, 2002.

[32] A. N. Chandran, S. Subba Rao, and Y. B. G. Varma, “Fluidized Bed Drying of Solids,” *AIChE J.*, vol. 36, pp. 29–38, 1990.

[33] E. K. Levy, H. S. Caram, Z. Yao, Z. Wei, and N. Sarunac, “Kinetics of coal drying in bubbling fluidized beds” *Proceedings Fifth World Congress on Particle Technology, Orlando, Florida*. 2006.

[34] W. Ciesielczyk and J. Iwanowski, “Analysis of Fluidized Bed Drying Kinetics on the Basis of Interphase Mass Transfer Coefficient,” *Dry. Technol.*, vol. 24, no. 9, pp. 1153–1157, Sep. 2006.

[35] S. Syahrul, I. Dincer, and F. Hamdullahpur, “Thermodynamic modeling of fluidized bed drying of moist particles,” *Int. J. Therm. Sci.*, vol. 42, no. 7, pp. 691–701, Jul. 2003.

[36] J. Cai and R. Liu, “Kinetic Analysis of Solid-State Reactions: A General Empirical Kinetic Model,” *Ind. Eng. Chem. Res.*, vol. 48, no. 6, pp. 3249–3253, Mar. 2009.

[37] T.-J. Kang, H. Namkung, L.-H. Xu, S. Lee, S. Kim, H.-B. Kwon, and H.-T. Kim, “The drying kinetics of Indonesian low rank coal (IBC) using a lab scale fixed-bed reactor and thermobalance to apply catalytic gasification process,” *Renew. Energy*, vol. 54, pp. 138–143, Jun. 2013.

[38] J. Burgschweiger, H. Groenewold, C. Hirschmann, and E. Tsotsas, “From hygroscopic single particle to batch fluidized bed drying kinetics,” *Can. J. Chem. Eng.*, vol. 77, no. 2, pp. 333–341, Apr. 1999.

[39] E. Mirzaee, S. Rafiee, and A. Keyhani, “Determining of moisture diffusivity and activation energy in drying of apricots,” vol. 2009, no. Yadollahinia 2006, pp. 114–120, 2009.

[40] R. G. Szafran and A. Kmiec, “CFD Modeling of Heat and Mass Transfer in a Spouted Bed Dryer,” *Ind. Eng. Chem. Res.*, vol. 43, no. 4, pp. 1113–1124, Feb. 2004.

[41] S. Azizi, S. H. Hosseini, M. Moraveji, and G. Ahmadi, “CFD modeling of a spouted bed with a porous draft tube,” *Particuology*, vol. 8, no. 5, pp. 415–424, Oct. 2010.

[42] T. J. Jamaleddine and M. B. Ray, “The Drying of Sludge in a Cyclone Dryer Using Computational Fluid Dynamics,” *Dry. Technol.*, vol. 29, no. 12, pp. 1365–1377, Sep. 2011.

[43] W. Sujanti and D. Zhang, “A laboratory study of spontaneous combustion of coal: the influence of inorganic matter and reactor size,” *Fuel*, vol. 78, no. 5, pp. 549–556, Apr. 1999.

[44] Z. Mao, H. Zhu, X. Zhao, J. Sun, and Q. Wang, “Experimental Study on Characteristic Parameters of Coal Spontaneous Combustion,” *Procedia Eng.*, vol. 62, pp. 1081–1086, 2013.

[45] Y. Yang, Z. Li, S. Hou, F. Gu, S. Gao, and Y. Tang, “The shortest period of coal spontaneous combustion on the basis of oxidative heat release intensity,” *Int. J. Min. Sci. Technol.*, vol. 24, no. 1, pp. 99–103, Jan. 2014.

[46] G. Qi, D. Wang, Y. Chen, H. Xin, X. Qi, and X. Zhong, “The application of kinetics based simulation method in thermal risk prediction of coal,” *J. Loss Prev. Process Ind.*, vol. 29, pp. 22–29, May 2014.

[47] X. Zhao, H. Xiao, Q. Wang, P. Ping, and J. Sun, “Study on spontaneous combustion risk of cotton using a micro-calorimeter technique,” *Ind. Crops Prod.*, vol. 50, pp. 383–390, Oct. 2013.

[48] “ASTM B311-13, Standard Test Method for Density of Powder Metallurgy (PM) Materials Containing Less Than Two Percent Porosity, ASTM International, West Conshohocken, PA, 2013, www.astm.org.”

[49] E. Azimi, “Simulation and performance characterization of air dense medium fluidized bed for coal beneficiation", PhD thesis, University of Alberta, 2014

[50] M. a. Hossain and B. K. Bala, “Thin-Layer Drying Characteristics for Green Chilli,” *Dry. Technol.*, vol. 20, no. 2, pp. 489–505, Feb. 2002.

[51] www.chemistry.about.com.

[52] C. J. Geankoplis, "Transport Processes and Separation Process Principles", Fourth ed. 2003.

[53] J. Crank," *The mathematics of diffusion*", 2nd edition. Oxford university press, 1975.

[54] S. R. Turns, "*An introduction to Combustion*", 3rd edition. McGraw.Hill, 2012, pp. 88–93.

[55] Petr A. Nikrityuk, B. Meyer, (Eds). "*Gasification Processes Modeling and Simulation"*. Wiley-VCH, p. 127.

[56] "ANSYS-FLUENT® Theory Guide, Release 14.0, 2013." .

[57] www.engineeringtoolbox.com. [Accessed: 15-Jun-2014].

[58] P. Lela, N. Ramesh, M. Raajenthiren, "A review of some existing drag models describing the interaction between the solid- gaseous phase in CFB," *Int. J. Eng. Sci. Technol.*, vol. 2, no. 5, pp. 1047–1051, 2010.

Appendix A: Calculating minimum fluidization

ρ_p =1400 kg/m^3

ρ_g =1.004 kg/m^3

μ_g =0.00001983

d_p =13 mm

using eq 2-3 we can write

$$Ar = \frac{\rho_g(\rho_p - \rho_g) g\, d_p^3}{\mu_g^2} = \frac{1.004(1400-1.004)*9.81*(0.0013)^3}{(o.oooo1983)^2} = 70659.2$$

Using eq 2-5:

$$Re_{mf} = 33.7[(1 + 3.59 * 10^{-5} Ar)^{0.5} - 1] = 29.6$$

Using eq 2-4:

$$u_{mf} = \frac{Re*\mu_g}{\rho_g d_p} = \frac{31.6*0.00001983}{1.004*0.00135} = 0.46\ m/s$$

Bed diameter =7 cm → Bed cross section area A= 38 cm^2

Air flow rate Q = u_{mf}. A=1.

5e-03 m^3/s = 90 lit/min